eNeuro

Research Article: New Research | Disorders of the Nervous System

Cellular and behavioral characterization of Pcdh19 mutant mice: subtle molecular changes, increased exploratory behavior and an impact of social environment

https://doi.org/10.1523/ENEURO.0510-20.2021

Cite as: eNeuro 2021; 10.1523/ENEURO.0510-20.2021

Received: 24 November 2020
Revised: 15 May 2021
Accepted: 24 June 2021

1. Manuscript title:
Cellular and behavioral characterization of *Pcdh19* mutant mice: subtle molecular changes, increased exploratory behavior and an impact of social environment.

2. Abbreviated title:
Pcdh19 mutant mice characterization

3. Author names and affiliations:
Natalia Galindo-Riera[1], Sylvia Adriana Newbold[1], Monika Sledziowska[1], Cristina Llinares-Benadero[1], Jessica Griffiths[1], Erik Mire[2], Isabel Martinez-Garay[1,*]

[1]Division of Neurosciences, School of Biosciences, Cardiff University, Cardiff CF10 3AX, UK
[2]Hodge Centre for Neuropsychiatric Immunology, Neuroscience and Mental Health Research Institute, Division of Psychological Medicine and Clinical Neurosciences, School of Medicine, Cardiff University, Cardiff CF24 4HQ, UK

4. Author Contributions:
IM-G and EM Designed Research; NG-R, SAN, MS, CLI-B, EM and IM-G Performed Research, NG-R, SAN, MS, CLI-B, JG, EM and IM-G Analysed Data; IMG wrote the paper with help from NG-R, SAN, MS, CLI-B, JG and EM.

5. Correspondence should be addressed to:
Isabel Martinez-Garay, Division of Neurosciences, School of Biosciences, Cardiff University, The Sir Martin Evans Building, Museum Avenue, Cardiff CF10 3AX.
Email: martinezgarayi@cardiff.ac.uk.
Tel: +44 (0)2922510029.

6. Number of Figures: 15 (8 main figures)
7. Number of Tables: 6
8. Number of Multimedia: 0
9. Number of words for Abstract: 155
10. Number of words for Significance Statement: 115
11. Number of words for Introduction: 694
12. Number of words for Discussion: 2742

13. Acknowledgements:
This work was supported by the Life Science Research Network Wales, an initiative funded through the Welsh Government's Ser Cymru program (fellowships to N.G-R. and J.G., initial fellowship to IM-G), the Wellcome Trust (Seed Award 109643/Z/15/Z to I.M-G., fellowship 204021/Z/16/A to S.A.N.), Cardiff University (Grant 501100000866 to M.S.) and the Hodge Foundation (Hodge Centre for Neuropsychiatric Immunology's fellowship to E.M.).
We would like to thank all members of the Martinez-Garay lab, as well as Y. Barde for insightful comments on this manuscript.
Current address for NG-R: Department of Medical Biochemistry and Biophysics, Karolinska Institute, 171 77 Stockholm, Sweden; Current address for MS: School of Biosciences, University of Birmingham, Birmingham, B15 2TT, UK; Current address for JG: UK Dementia Research Institute, Imperial College London, London, W12 0NN, UK and UK Dementia Research Institute, University of Edinburgh, Edinburgh, EH16 4SB, UK.

14. Conflict of Interest:
Authors report no conflict of interest

Cellular and behavioral characterization of *Pcdh19* mutant mice: subtle molecular changes, increased exploratory behavior and an impact of social environment.

ABSTRACT

Mutations in the X-linked cell adhesion protein PCDH19 lead to seizures, cognitive impairment and other behavioral comorbidities when present in a mosaic pattern. Neither the molecular mechanisms underpinning this disorder, nor the function of PCDH19 itself are well understood. By combining RNA *in situ* hybridization with immunohistochemistry and analyzing single cell RNAseq datasets, we reveal *Pcdh19* expression in cortical interneurons and provide a first account of the subtypes of neurons expressing *Pcdh19*/*PCDH19*, both in the mouse and the human cortex. Our quantitative analysis of the *Pcdh19* mutant mouse exposes subtle changes in cortical layer composition, with no major alterations of the main axonal tracts. In addition, *Pcdh19* mutant animals, particularly females, display preweaning behavioral changes, including reduced anxiety and increased exploratory behavior. Importantly, our experiments also reveal an effect of the social environment on the behavior of wild-type littermates of *Pcdh19* mutant mice, which show alterations when compared with wild-type animals not housed with mutants.

SIGNIFICANCE STATEMENT

PCDH19 mutations cause epileptic encephalopathy in humans, but the underlying pathophysiology is not completely understood. Here, we provide the first quantitative analysis of the cortical neuronal types expressing *Pcdh19* in the mouse and human neocortex, and of cortical layer composition in *Pcdh19* mutant animals, revealing expression of *Pcdh19* in interneurons and the presence of small, but significant changes in neuronal distribution. The findings of our behavioral analysis indicate not only reduced anxiety and increased exploratory behavior, but also an impact of the mutant genotype on the behavior

of wild-type animals when housed in the same cage. This finding underscores the importance of selecting appropriate control cohorts to avoid missing relevant behavioral changes in mutant animals.

INTRODUCTION

PCDH19 is one of several genes located on the X chromosome known to impact neurodevelopment and behavior. Mutations in this gene were identified in patients suffering from EIEE9 (Epileptic Encephalopathy, Early Infantile, 9, OMIM #300088), also known as Girls Clustering Epilepsy (GCE), over a decade ago (Dibbens et al., 2008). Since then, more than 140 mutations have been described (Kolc et al., 2018), consolidating *PCDH19* as the second most relevant gene in epilepsy after *SCNA1* (Depienne and Leguern, 2012; Duszyc et al., 2015). The pathogenicity of *PCDH19* mutations is dependent on cellular mosaicism and therefore the disorder follows an unusual inheritance, manifesting in heterozygous females and in males with somatic mutations (Depienne et al., 2009; Terracciano et al., 2016). Affected patients develop symptoms during early infancy, often within their first year of life, and display clustered seizures, varying degrees of cognitive impairment and other comorbidities, including autism spectrum disorder, attention deficits and obsessive-compulsive features (Kolc et al., 2020).

PCDH19 codes for Protocadherin 19, a calcium-dependent cell-cell adhesion molecule of the cadherin superfamily. This delta 2 protocadherin has 6 extracellular cadherin repeats, a single transmembrane domain and a cytoplasmic tail with two conserved motives of unknown function (CM1 and CM2, (Wolverton and Lalande, 2001)). In addition, a WRC interacting receptor sequence (WIRS) downstream of CM2 allows PCDH19 to interact with the WAVE regulatory complex, enhancing its Rac1-mediated activation (Chen et al., 2014). PCDH19 is involved in different processes, ranging from neurulation and organization of the optic tectum in zebrafish (Emond et al., 2009; Cooper et al., 2015) to neurogenesis and regulation of GABAergic transmission in mammals (Fujitani et al., 2017; Bassani et al., 2018;

Homan et al., 2018; Lv et al., 2019; Serratto et al., 2020). In addition, PCDH19 is involved in gene expression regulation with estrogen receptor alpha (Pham et al., 2017) and mutations in *PCDH19* lead to a deficiency of the neurosteroid allopregnanolone and of other neuroactive steroids (Tan et al., 2015; Trivisano et al., 2017). Two very recent publications have also addressed the role of PCDH19 in synapse formation in hippocampal cells (Mincheva-Tasheva et al., 2021; Hoshina et al., 2021).

To date, three different *Pcdh19* knockout (KO) mouse models have been developed to explore the function of PCDH19. The first, produced by Taconic Biosciences, has the first three exons of the gene replaced by a beta galactosidase and neomycin (*LacZ-neo*) resistance cassette (Pederick et al., 2016). The second model retains exons 2 and 3, with a *LacZ-neo* selection cassette replacing exon 1, which encodes the entire extracellular and transmembrane domains (Hayashi et al., 2017). The third was created by CRISPR-Cas9-mediated deletion of exon 1 (Hoshina et al., 2021). Lack of *Pcdh19* mRNA and protein was confirmed for two of the models (Pederick et al., 2016; Hoshina et al., 2021) and no major anatomical defects were reported in either of the three mutant animal lines. However, increased neuronal migration has been described (Pederick et al., 2016), as well as behavioral alterations (Hayashi et al., 2017; Lim et al., 2019; Hoshina et al., 2021). In addition, heterozygous females display a striking segregation of *Pcdh19* expressing and non-expressing progenitors in the developing cortex and altered electrocorticogram traces (Pederick et al., 2018), as well as presynaptic defects in the hippocampal mossy fiber synapse that lead to long term potentiation (LTP) abolishment (Hoshina et al., 2021). Although no major abnormalities in cortical architecture have been reported in either KO mouse model, no detailed, quantitative analysis has been carried out yet. Similarly, while RNA *in situ* hybridization (ISH) revealed strongest *Pcdh19* expression in layers II/III and V(a) in mice (Pederick et al., 2016; Hayashi et al., 2017), the neuronal subtypes expressing *Pcdh19* have not been characterized, possibly due to the difficulty of labeling PCDH19 expressing cells with current antibodies. Here we report on the identity of *Pcdh19* expressing excitatory and inhibitory neurons in the mouse and human cortex, focusing mainly on

somatosensory areas. We also uncover alterations in cortical neuronal distribution in the somatosensory cortex of Taconic *Pcdh19* mutant animals, as well as robust differences in the behavior of heterozygous females, including preweaning alterations and an impact of mutant animals on the behavior of their wild type littermates.

MATERIAL AND METHODS

Experimental animals

Animals were housed under a 12 h light/dark cycle with *ad libitum* access to water and food, and controlled temperature and humidity. All experiments using mice were approved by the local ethical boards and carried out following the directions of the UK Animal Scientific Procedures Act (update 1986).

C57BL6/J wild-type (WT) animals were purchased from Charles River Laboratories and the *Pcdh19* knock-out (KO) line (TF2108) was acquired from Taconic Biosciences. Experimental matings for anatomical and cellular characterization, as well as for behavioral analysis were set up using wild type males and *Pcdh19* heterozygous (HET) females to produce litters with WT males and females, KO males and HET females.

Analysis of single cell RNAseq datasets

Gene expression matrices and metadata were downloaded from https://portal.brain-map.org/atlases-and-data/rnaseq. Analysis and visualization were carried out using R v.3.6.3, assisted by RStudio v.1.2.1335. Raw counts were normalised to account for library size (total sum of counts per cell) and transformed to counts per million (CPM) using R package scater v.1.16.2. Violin plots were generated with R packages gridExtra v.2.3 and ggplot2 v.3.3.1. River plots were made with R packages gridExtra v.2.3, ggplot2 v.3.3.1 and ggforce v.0.3.2.

Tissue processing

Animals were perfused with PBS followed by 4% paraformaldehyde (PFA) in PBS. After perfusion, brains were extracted and post-fixed in PFA 4% overnight at 4 °C. For RNA ISH, brains were then cryoprotected in 30% sucrose in PBS before embedding in OCT compound (Tissue-Tek) prior to freezing. Samples were stored at -80 °C until sectioning. 12 or 20 µm sections were cut with a cryostat (CM3050, Leica Systems) and stored at -80 °C until use. For immunostaining, fixed brains were briefly washed in PBS and embedded in 4% low melting point agarose. 50 µm sections were cut with a vibrating microtome (VT1000S, Leica Systems) and stored in PBS with 0.05% sodium azide at 4 °C until use.

RNA *in situ* hybridization and immunohistochemistry

The probe to detect *Pcdh19* has been described before (Gaitan and Bouchard, 2006). Its sequence was amplified using primers Pcdh19e1-F, 5'-CACCAAGCAGAAGATTGACCGAG-3' and Pcdh19e1-R, 5'-GCCTCCCATCCACAAGAATAGTG-3' and cloned into pCRII-Blunt-TOPO (Invitrogen). This plasmid was then used to generate digoxigenin-labeled sense and antisense probes.

Thawed sections were post-fixed in 4% PFA, endogenous peroxidases were quenched with 3% hydrogen peroxidase and slices were then acetylated in a 0.25% acetic anhydride solution. Pre-hybridization took place in pre-warmed hybridization buffer (50% formamide, 0.1% Tween-20, 0.25% CHAPS, 250 µg/ml yeast tRNA, 500 µg/ml herring sperm, 5x Denhardts, 5x SSC, 50 µg/ml heparin, 2.5 mM EDTA) for 1h at 65 °C. Slices were hybridized with the denatured sense or antisense probes overnight at 65 °C in a humidified chamber. The next day, slides were washed with 0.2X SSC (GIBCO) and PBST, and then blocked in ISH blocking solution (10% DS and 0.1% TritonX-100 in PBS) for 20 min at RT. After blocking, brain slices were incubated in primary antibody for 1 h at RT; washed in PBST and incubated in secondary antibody for 1 h at RT. Antibodies used are described below. Slides were then washed in PBST, equilibrated in TN buffer (150 mM NaCl and 100 mM Tris pH= 7.5 in water) and incubated for 30 min in 1:2000 HRP-coupled anti-DIG antibody (Sigma-

194 Aldrich, 11207733910). Following the incubation, tissue was rinsed in TNT (TN + 0.5%
195 Tween) and immersed in Cy3-Tyramide (TSATM Plus Cy3 Fluorescence kit, Perkin-Elmer,
196 NEL744001KT) in a 1:50 dilution dissolved in the amplification diluent. Slides were then
197 washed, counterstained with DAPI and mounted in DAKO.
198
199 **Immunohistochemistry**
200 Antigen retrieval was performed for stainings with antibodies against RORB, SATB2, Pvalb
201 and CR, with the tissue either immersed in a 10 mM citrate buffer pH = 6, at 95 °C for 5 min
202 (RORB and SATB2) or 10 min (Pvalb, CR) before blocking. 50 µm coronal sections were
203 blocked (4% BSA, 3% donkey serum, 0.1% Triton X-100 in PBS) at RT for 1 h. The tissue
204 was then incubated in primary antibody diluted in blocking solution overnight at 4 °C.
205 Primary antibodies used for immunostaining were as follows: anti-CUX1 rabbit polyclonal
206 (1:200; Proteintech, 11733 or Santa Cruz Biotechnology, sc-13024), anti-CTIP2 rat
207 monoclonal (1:250; Abcam, ab18465), anti-SATB2 mouse monoclonal (1:400; Abcam,
208 ab51502), anti-RORB rabbit polyclonal (1:200; Proteintech, 17635-1AP), anti-TBR1 rabbit
209 polyclonal (1:350; Abcam, ab31940), anti-Pvalb rabbit polyclonal (1:10000 or 1:500 for ISH;
210 Swant, PV27), anti-CB rabbit polyclonal (1:5000; Swant, CB38), anti-CR mouse polyclonal
211 (1:1000; Merck, AB5054), anti-SST rat monoclonal (1:200; Merck, MAB354), anti-L1CAM rat
212 monoclonal (1:500, Merck, MAB5272), anti-Neuropilin1 goat polyclonal (1:300, R&D
213 Systems, AF566).
214 Slices were then rinsed in PBS and incubated with secondary antibodies coupled to
215 fluorochromes (Alexa Fluor range, Thermo Fisher Scientific) for 1 h at RT. Nuclei were
216 counterstained with DAPI for 10 min, washed again in PBS and mounted with DAKO
217 mounting medium.
218
219 **Image acquisition and analysis**
220 Images were acquired using a confocal laser scanning microscope (LSM 780, Carl Zeiss)
221 and ZEN Black software (version 2.0, Carl Zeiss). Image analysis was conducted with

ImageJ Fiji software (Schindelin et al., 2012). For quantification, the cortical wall was divided into ten horizontal bins of equal width. The number of marker positive cells in each bin was quantified and is shown as mean percentage relative to the total number of cells in all ten bins, ± standard error of the mean (SEM).

Behavioral analysis

Behavioral tests were conducted at P21 (pre-weaning) and in young adults (P60 and over). Two different WT controls were tested: WT littermates of the mutant animals (mixed genotyped housing mice, MGH) and animals from pure WT litters (single genotype housed mice, SGH). The WT parents of the SGH animals were derived from the *Pcdh19* colony. Mice were habituated to the new environment by taking them to the behavioral room 30 min prior to the tests. Mice were handled with open hands to reduce anxiety levels and a maximum of one behavioral test was performed per day.

Open field

Open field behavioral analysis was performed on two consecutive days, using the first day to habituate the mice to the new environment. Mice were allowed to explore freely, in the dark, for 20 min, in an open field arena (40 cm x 40 cm). Spontaneous locomotion was recorded using a computer-linked video camera (The Imaging Source) located above the arena and an infrared illumination box (Tracksys) located underneath the arena. The EthoVision XT software (Noldus) was used to analyze total distance travelled, distance travelled in intervals of 5 min and time spent in the center of the arena. The center of the arena was defined as the area separated from the wall by 5 cm or more.

Elevated plus maze

Each mouse was left to explore freely for 5 min in a maze consisting of 4 perpendicular arms (40 cm x 7 cm): two open arms (1 cm high) and two closed arms (16 cm high), in a well-lit room. Behavior was recorded using a computer-linked video camera (The Imaging Source)

250 located above the maze. Total time spent in the open arms was measured using EthoVision
251 XT software (Noldus).
252
253 **Social interaction**
254 At P21, test pups were habituated to the arena for 3 min. Subsequently, WT females in
255 estrous, unfamiliar to the pups, were added to the cage and both mice were allowed to
256 interact with each other for another 3 min in a well-lit room. The interaction between the
257 pups and the females was recorded using a computer-linked video camera (The Imaging
258 Source) located above the arena. Videos were manually scored, and interaction recorded
259 when both mice were within 2 cm of each other, not including tail-tail interactions.
260 At P60, only female mice were tested for social interaction. In this case the unknown WT
261 females were not required to be in oestrus.
262 To determine which females were in oestrus, vaginal smears were stained with Giemsa
263 solution (Polysciences inc.) (Caligioni, 2009) prior to the experiment.
264
265 **24-hour activity**
266 P60 experimental mice were placed in individual clear boxes (40 cm x 24 cm x 18 cm) and
267 let to roam free for 24 h with *ad libitum* access to food and water and their normal 12 h
268 light/dark cycle. Three infrared beams traversed each cage at the bottom. Data were
269 analyzed using the MED-PC® IV software suite and extracted using the MPC2XL program.
270 The number of beams breaks in 24 h and in 1 h slots, as well as the total number of beam
271 breaks during the light and dark periods were analyzed.
272
273 **Experimental design and statistical analysis**
274 For all experiments, individual animals were considered the experimental unit and data
275 obtained from each animal was averaged if more than one quantification was performed (for
276 example when analysing several brain slices from the same animal). Experimenters were
277 blind to the genotype of the animals until all quantification or scoring was completed.

Statistical analysis was performed using GraphPad Prism (version 9) (cortical lamination analysis) or R software (behavior), version 3.6.2. (R Core Team 2019). Normality of the data was tested using the Shapiro-Wilk test and homogeneity of variance was assessed with Levene's test. If either assumption was violated an appropriate non-parametric test was used. Comparisons between two groups were performed using a 2-tailed independent sample t-test for normal data, or a Mann-Whitney test if data distribution did not meet normality criteria. If the variance of the two groups differed, a Welch correction was applied. For comparison of more than two groups, analysis of variance (ANOVA) was used for normal data and Kruskal-Wallis if the assumption of normality was not met. If only the assumption of homogeneity of variance was not met, a Welch's ANOVA test was used. Post-hoc test following ANOVA was adjusted according to Tukey's HSD or, in the case of the social interaction analysis, Dunnet's test. Kruskal-Wallis was followed by Dunn's correction and Welch's ANOVA was followed by Games-Howell correction. Statistical data are presented as mean ± SEM for formal tests. To carry out estimation statistics for the behavioral experiments, data were introduced into the form available at www.estimationstats.com, in the section for multiple two-groups to obtain the mean differences between groups and their corresponding 95% confidence intervals (CIs). Y-axis limits were set for the optimal display of the raw data, and the graphs obtained were directly used in the figures of the manuscript. Calculation of the unbiased Cohen's *d* for each comparison, as well as its 95% CI was carried out using the esci module on jamovi (The jamovi project (2021). jamovi (Version 1.6) [Computer Software]. Retrieved from https://www.jamovi.org).

RESULTS

Pcdh19 is expressed by different subtypes of cortical projection neurons and interneurons

Previous RNA *in situ* hybridization (ISH) studies have shown two main areas of *Pcdh19* expression in the adult cortex, corresponding to the upper regions of layer V (layer Va) and II/III (Hertel and Redies, 2010; Pederick et al., 2016). However, a detailed analysis of the cortical neuronal subtypes expressing *Pcdh19*, an important consideration given the cellular diversity of the cortex, is still lacking. To address this question, ISH against *Pcdh19* was combined with immunohistochemistry (IHC) against several cortical markers for principal neurons and interneurons in the somatosensory cortex at postnatal days 10 (P10) and P20, respectively (Fig. 1 A-D). At P10, *Pcdh19*+ cells were found to co-express markers for layer IV neurons (RORB, Fig. 1A), callosal projection neurons (SATB2, Fig. 1B), corticospinal neurons (CTIP2, Fig. 1B), and corticothalamic neurons (TBR1, Fig. 1C). Strongest co-expression was seen in SATB2+ neurons, whereas RORB+ cells showed weaker expression and in a smaller proportion of cells. CTIP2+ neurons with strong *Pcdh19* expression tended to be located in the upper half of layer V, whereas TBR1+ cells co-expressing *Pcdh19* did so at generally lower levels. At P20, we identified interneurons co-expressing *Pcdh19* with Parvalbumin in layers II/III and V (Fig. 1D), as well as double positive cells for Calbindin and *Pcdh19* (data not shown). These data suggest that in juvenile animals *Pcdh19* is expressed in both intratelencephalic and corticofugal projection neurons and reveal a previously unreported expression in subpopulations of cortical interneurons.

The previous approach does not allow the identification of distinct molecular subtypes of excitatory and inhibitory neurons populating the neocortex. We thus turned to publicly available datasets of cortical single cell RNA expression to ascribe molecular identities to *Pcdh19* expressing neurons in the mouse adult somatosensory cortex. We chose the "Whole Cortex & Hippocampus - SMART-SEQ (2019) with 10X-Smart-Seq Taxonomy (2020)" dataset from the Allen Brain Atlas (available at https://portal.brain-map.org/atlases-and-data/rnaseq) that includes 76,307 single-cell transcriptomes with cluster-assigned

identity isolated from a total of 21 adult cortical and hippocampal regions, including primary and secondary somatosensory cortex. The 74,973 cells for which metadata are available in this dataset are classified into 379 cell types, of which 236 are glutamatergic, 119 GABAergic and 24 non-neuronal (Yao et al., 2020). We filtered for neurons originating from the primary (SSp) and supplemental (SSs) somatosensory cortex using the dataset metadata, which yielded a total of 7,303 neurons (Fig. 1E). Those neurons are assigned to 19 subclasses (Fig. 1F), although 4 of them contain less than 10 cells (Meis2 (5 cells), L2 IT RHP (4 cells), L5 IT TPE-ENT (3 cells) and L2/3 IT CTX-2 (2 cells)) and have not been included in the figure. Our analysis shows that, in agreement with our P10 and P20 results, *Pcdh19* expression is maintained in both excitatory and inhibitory populations in the adult somatosensory cortex that co-express the markers of our ISH analysis (Fig. 1E-H).

In excitatory neurons of the adult somatosensory cortex, *Pcdh19* expression is lowest in the L6 IT CTX and L6 Car subclasses, where all clusters show consistent low median expression. However, in the remaining subclasses there is always at least one cluster that shows higher expression, indicating that there are *Pcdh19* expressing neuronal populations in layer II/III and layer V, but also in layers VI and VIb, and possibly in layer IV, matching the results of our ISH analysis (Fig. 1G). The neurons expressing *Pcdh19* and SATB2 in layers II/III that we identified at P10 (Fig. 1B) could potentially represent clusters 178 and 182 of L2/3 intratelencephalically (IT) projecting neurons. In layer V, neurons expressing *Pcdh19* and CTIP2 may correspond to clusters 250 and 251, representing layer V neurons that project outside the cortex (PT), and/or clusters 304-306 of near projecting neurons (NP), whereas those expressing *Pcdh19* and SATB2, but not CTIP2, would be layer V IT neurons, matching those in clusters 190-192, 200 and 207. We also identified neurons expressing *Pcdh19* and TBR1 in layer VI (Fig. 1C) that could be corticothalamic neurons (clusters 323, 325 and 327) or layer VIb neurons (clusters 339 and 348-350).

A comparison between different brain regions (Fig. 1-1) shows that, although expression levels in the different clusters are generally conserved across brain regions, there are also marked variations in several clusters that tend to manifest in just one or two specific regions.

As in the case of projection neurons, *Pcdh19* expression in interneurons of the adult somatosensory cortex is strongly cluster dependent. More specifically, strongest average expression is found in the *Sst-Chodl* and *Pvalb* subclasses (Fig. 1F); however, there is considerable variation and several *Sncg*, *Vip* and *Sst* clusters also express *Pcdh19* widely (Fig. 1H). To assign more meaningful identities to the interneuronal clusters expressing *Pcdh19*, we made use of the correlation provided between the GABAergic clusters generated from this dataset and the previous taxonomy from Tasic et al 2018 (Yao et al., 2020). *Sncg* neurons are *Vip*+, *Cck*+ multipolar or basket cells located mainly in upper layers, and 2 out of their 4 subtypes have consistent *Pcdh19* expression. Three clusters of *Vip* interneurons also show relevant *Pcdh19* expression (Vip clusters 47, 51 and 59), with at least one of them corresponding to bipolar or multipolar cells (47_Vip). Within the *Pvalb* subclass, *Pcdh19* is expressed by Chandelier cells (119_Pvalb Vipr2) and several subtypes of basket cells (Pvalb clusters 112 - 116). Finally, within the *Sst* subclass, *Pcdh19* expression is strongest in some subtypes of upper layer basket and Martinotti cells (Sst clusters 94 and 95), and in the long-range projecting population (61_Sst-Chodl). Again, variations in the level of *Pcdh19* expression within GABAergic clusters can be seen between brains regions (Figure 1-2), but, as was the case for excitatory neurons, differences tend to be limited to a few regions per cluster.

In summary, our analysis demonstrates that mouse *Pcdh19* expression is cluster-specific in all glutamatergic and GABAergic subclasses in the somatosensory cortex and other cortical areas, being expressed by a heterogeneous neuronal population that includes discrete subtypes of cortical projection neurons and interneurons, with some variation between brain areas. Expression in non-neuronal cells is very low (data not shown).

Human *PCDH19* is also expressed in excitatory and inhibitory neurons

Mutations in *PCDH19* cause severe impairments in brain function, yet the expression profile in human cortical neurons is unclear. We therefore extended our analysis to a publicly available human dataset from the Allen Brain Atlas (Human – Multiple Cortical Areas –

SMART-seq, available at https://portal.brain-map.org/atlases-and-data/rnaseq), obtained from several brain areas (middle temporal gyrus, anterior cingulate gyrus, primary visual cortex, primary motor cortex, primary somatosensory cortex and primary auditory cortex). This dataset comprises 49,417 cell nuclei (metadata available for 47,432) and has allowed the definition of 56 excitatory and 54 inhibitory subtypes. We applied the same strategy as with the mouse dataset, filtering for those neurons originating in the somatosensory cortex, which reduced the dataset to 5,103 neurons ascribed to 12 subclasses (Fig. 2A,B). Analysis of *PCDH19* expression in this restricted dataset revealed that, within glutamatergic neurons, *PCDH19* is primarily expressed in several excitatory neuronal subtypes, particularly Exc L5 FEZF2 SCN7A, which contains layer V neurons that project outside the cortex, and a series of clusters of intracortically projecting neurons spanning layers II-V, such as Exc L3 RORB CARTPT, Exc L3-4 RORB FOLH1B, Exc L5 RORB SNHG7 and Exc L4-5 RORB LCN15 (Fig. 2C). Low expression is evident in many other excitatory neurons of layers III-VI, although several layer IV and VI clusters tend to express much lower levels of *PCDH19*. A comparison between different brain regions beyond the SSC shows good correlation between the levels of *PCDH19* expression within clusters, with only few exceptions (Fig. 2-1). Regarding interneurons, *PCDH19* expression is highest in the L3-6 VIP KCTD13 subtype, with strong expression in most cells. In addition, *PCDH19* is also relatively highly expressed in several other VIP, LAMP5, SST and PVALB subpopulations (Fig. 2D). A comparison between different brain regions reveals that, in general, *PCDH19* is expressed in each cluster at similar levels across areas. However, there are some exceptions, like L1 VIP PCDH20 interneurons, which show much higher *PCDH19* expression in the visual cortex (V1C) than in somatosensory areas (S1lm and S1ul) or L1-2 VIP RPL41P3, with higher *PCDH19* expression in motor areas (Fig. 2-2).

Having determined the levels of *Pcdh19/PCDH19* expression in the different clusters of excitatory and inhibitory neurons in mouse and human SSC, we set out to evaluate whether expression levels are correlated between clusters in the two species, a relevant issue when using the mouse to investigate a human disorder. No direct equivalents have been

418 described for the clusters of these two datasets, so we took an indirect route, using
419 additional information from the metadata of the Mouse V1 & ALM - SMART-SEQ (2018) and
420 Human MTG - SMART-SEQ (2018) datasets (both available at https://portal.brain-
421 map.org/atlases-and-data/rnaseq) (Fig. 2-3A). This analysis was only possible for
422 GABAergic neurons, as their clusters (but not the glutamatergic ones) have been correlated
423 between the Whole Cortex & Hippocampus - SMART-SEQ (2019) with 10X-Smart-Seq
424 Taxonomy (2020) and the Mouse V1 & ALM - SMART-SEQ (2018) datasets (Yao et al.,
425 2020). We first determined the composition of the homologous cell types described for these
426 additional mouse and human datasets (Hodge et al., 2019) (Fig. 2-3B), and then the
427 correlation between the human MTG and Multiple Brain Areas clusters (Fig. 2-3C). This
428 allowed us to establish an indirect comparison between the clusters with highest
429 *Pcdh19/PCDH19* expression in mouse and human SSC (Table 1). In general, there is a
430 relatively good correlation between the clusters with highest *Pcdh19* expression, particularly
431 for the 3_Lamp Lhx6 cluster, which seems to correspond to Chandelier cells in layers V/VI
432 (Chandelier type 2 cells, Paul et al., 2017; Tasic et al., 2018), most (but not all) of the *Vip*
433 clusters and several *Pvalb* clusters, including the Chandelier cells of 110_Pvalb Vipr2.
434 Correlation in the *Sst-Chodl* subclass is lower, with mouse long projecting interneurons
435 expressing higher levels of *Pcdh19* than their human counterparts. Levels of expression in
436 clusters of the *Sst* subclass also tend to show higher variability between the two species.
437
438 **Subtle changes in layer composition in *Pcdh19* mutant animals**
439 Although no major morphological defects have been described in *Pcdh19* mutant brains
440 (Pederick et al., 2016; Hayashi et al., 2017), a detailed, quantitative study of cortical
441 lamination hasn't been performed so far. Given that *Pcdh19* is expressed in projection
442 neurons and interneurons, we performed an analysis with markers for both neuronal
443 populations in the somatosensory cortex. We first selected cortical markers for projection
444 neurons of deep and upper layers (CUX1, SATB2, RORB, CTIP2 and TBR1) and performed
445 immunohistochemistry at P10, once radial migration is completed. For each marker, we

446 determined the proportion of positive cells, as well as their distribution within 10 bins
447 covering the whole width of the cortical plate. We analyzed males and females separately,
448 using WT male controls (WT-M) for the KO males and WT female controls (WT-F) for the
449 HET animals (except for CUX1, where this was not possible for technical reasons).
450 In accordance with previous reports (Pederick et al., 2016), we found no differences in
451 cortical width between genotypes (WT-M average = 1381.47 ± 33.72 µm, KO = 1309.10 ±
452 32.07 µm, WT-F = 1346.85 ± 39.67 µm, HET = 1348.47 ± 32.46 µm; Fig. 3A; Table 2[a]). The
453 proportion of positive neurons for all five examined markers was also unaltered (Fig. 3B,C;
454 Table 2[b-f]). CUX1+ cells made up approximately one fifth of all DAPI+ cells (WT = 21.24 ±
455 1.32%, HET = 22.34 ± 1.64%, KO = 24.66 ± 2.05%) and SATB2+ cells represented more
456 than half of all cells (WT-M = 62.20 ± 4.09%, KO = 58.95 ± 2.45%, WT-F = 63.01 ± 2.78%,
457 HET = 57.96 ± 3.64%). The proportion of RORB+ cells seemed lower in KO brains
458 compared to WT-M brains (WT-M = 28.96 ± 0.50%, KO = 18.86 ± 3.74%, WT-F = 27.86 ±
459 2.15%, HET = 24.37 ± 2.49%), but statistical analysis revealed this difference was not
460 significant (Mann-Whitney, $U = 3$, $P = 0.2$). CTIP2+ cells were also equally abundant among
461 the four groups (WT-M = 19.97 ± 3.94%, KO = 13.58 ± 1.15%, WT-F = 18.81 ± 3.16%, HET
462 = 15.89 ± 2.46%) and TBR1+ cells added up to approximately one third of all cells (WT-M =
463 32.40 ± 2.26%, KO = 38.43 ± 1.80%, WT-F = 35.21 ± 2.40%, HET = 33.85 ± 2.64%).
464 The distribution of SATB2+ neurons between the 10 bins was unchanged for males and
465 females (Fig. 3G-J). However, we detected some deviations in the distribution of CUX1+,
466 CTIP2+, RORB+ and TBR1+ neurons (Fig. 3D-L). Regarding CUX1, the difference was
467 apparent in bin 5 (Fig. 3E). *Pcdh19*-HET animals showed a significant 2.4-fold reduction in
468 the percentage of CUX1+ neurons in this bin compared to wild types (WT = 2.08 ± 0.18%,
469 HET = 0.86 ± 0.27%, KO = 1.14 ± 0.32%; one way ANOVA, $F(2,9) = 5.81$, $P = 0.0239$;
470 Tukey: $q(1,9) = 4.60$, $P = 0.0245$ HET vs WT). For CTIP2, we found differences in bins 3
471 (1.7-fold increase) and 7 (1.6-fold reduction) in KO males, suggesting a redistribution of
472 CTIP2+ neurons to higher positions in layer V (Bin 3: WT-M = 2.76 ± 0.37%, KO-M = 4.17 ±
473 0.34%; independent t-test, $t(2, 6) = 2.787$, $P = 0.0317$; Bin 7: WT-M = 16.74 ± 1.67%, KO-M

= 10.68 ± 0.34%; independent t-test with Welch correction for unequal variance, t = 3.556, P = 0.0333). HET females showed double the percentage of cells in bin 1 than their WT siblings (WT-F = 2.20 ± 0.29%, HET-F = 4.42 ± 0.29%; independent t-test, $t(2, 6)$ = 5.391, P = 0.0017) (Fig. 3D,F). Differences in RORB+ distribution were only present in males, specifically in bin 2, with a 3.4-fold reduction (WT-M = 11.38 ± 2.00%, KO-M = 3.36 ± 2.37%; independent t-test, $t(2, 6)$ = 2.585, P = 0.0415; Fig. 3G,H). However, the graphs for KO and HET animals suggest that the distribution of RORB+ cells tended to be more condensed in those animals. Finally, KO males showed a 2.4-fold increase in the percentage of TBR1+ cells in bin 1 compared with their WT counterparts (WT-M = 1.77 ± 0.33%, KO-M = 4.50 ± 0.33%; independent t-test, $t(2, 6)$ = 5.818, P = 0.0011), and HET females had a 1.4-fold reduction in the percentage of TBR1+ cells in bin 3 (WT-F = 15.98 ± 0.58%, HET-F = 11.10 ± 0.92%; independent t-test, $t(2, 6)$ = 4.473, P = 0.0042) and a 1.6-fold increase in bin 5 (WT-F = 4.62 ± 0.79%, HET-F = 7.46 ± 0.35%; independent t-test, $t(2, 6)$ = 3.268, P = 0.0171) (Fig. 3K,L). A comparison between WT males and females did not reveal any differences in the distribution of the 4 markers analyzed for excitatory neurons (data not shown).

To complete our analysis on cortical composition and lamination, we stained the SSC with four different interneuronal markers (SST, PVALB, CB, and CR) in P20 brains. As before, cortical thickness showed no difference between genotypes of matched gender (WT-M average = 1424.49 ± 57.19 µm, KO = 1387.02 ± 9.88 µm, WT-F = 1429.61 ± 48.84 µm, HET = 1402.97 ± 42.92 µm; Fig. 4A; Table 3[a]). However, in this case, some differences were apparent in the overall proportion of three types of interneurons, which may be due in part to the smaller number of cells that test positive for these markers (Fig. 4B; Table 3[b-e]). The most abundant type was CB+ cells (WT-M = 18.91 ± 1.20%, KO = 18.77 ± 0.20%, WT-F = 14.19 ± 0.98%, HET = 16.20 ± 1.21%), that despite no changes between genotypes within males or females, displayed a significantly lower proportion in WT females than in WT males (unpaired t-test, $t(2, 6)$ = 3.054, P = 0.0224). PVALB+, SST+ and CR+ accounted for less than 5% of DAPI+ cells each (Fig. 4B). The proportion of PVALB+ interneurons was very

similar across the 4 groups (WT-M = 3.16 ± 0.33%, KO = 3.15 ± 0.21%, WT-F = 4.06 ± 0.55%, HET = 3.70 ± 0.20%), but HET females showed a slight decrease in SST+ cells (WT-M = 2.31 ± 0.23%, KO = 1.61 ± 0.33%, WT-F = 2.19 ± 0.31%, HET = 1.34 ± 0.11%; unpaired t-test, $t(2, 6) = 2.578$, $P = 0.0419$ WT-F vs HET) and KO males a similarly small decrease in CR+ interneurons (WT-M = 1.98 ± 0.39%, KO = 0.98 ± 0.10%, WT-F = 1.63 ± 0.24%, HET = 1.14 ± 0.04%; unpaired t-test, $t(2, 6) = 2.509$, $P = 0.0459$ WT-M vs KO).

Regarding cellular distribution in the SSC, no differences were apparent for CB+ cells in KO males or HET females (Fig. 4C-F). However, we detected changes in the distribution of SST+ (HET females), CR+ (KO males) and PVALB+ (HET females) interneurons (Fig. 4C-J). HET brains displayed a 1.6-fold increase in the percentage of SST+ cells in bin 8 when compared to gender matched WT brains (WT-F = 10.13 ± 1.15%, HET-F = 15.79 ± 0.4%; independent t-test, $t(2, 6) = 4.647$, $P = 0.0035$, Fig. 4E,F). Although not significant due to higher variability, bin 9 also reflects an increase in SST+ interneurons in HET brains, whereas bins 2 and 3 seem to have reduced numbers, suggesting a potential redistribution of SST+ cells towards deeper layers in HET females. Changes in CR+ cell distribution were found in bin 8 of KO brains, which displayed a roughly 2-fold reduction over WT male brains (Bin 8: WT-M = 8.16 ± 0.57%, KO-M = 4.06 ± 1.05%; Mann-Whitney, $P = 0.0286$, Fig. 4G,H). This change, combined with another decrease in bin 7 and concomitant increases in bins 2 and 3 that did not reach statistical significance, might indicate a tendency of CR+ interneurons to occupy higher positions within the cortex in KO animals. As for PVALB+ cells, HET brains showed a reduced percentage in bin 8 (WT-F = 11.54 ± 0.96%, HET-F = 8.61 ± 0.44%; independent t-test, $t(2, 6) = 2.777$, $P\ p = 0.0321$, Fig.4 I,J). In this case, some differences were found in the distribution of CB+ (Bin 4), CR+ (bin 8) and PVALB+ (bin 7) interneurons between WT males and females (data not shown, but see discussion).

In summary, despite relative neuronal proportions and distribution being mostly normal in the SSC of *Pcdh19* mutant animals, subtle but significant differences in distribution are apparent for many of the analyzed neuronal markers.

No obvious defects in axonal tracts in *Pcdh19* mutant animals

Our results indicate that *Pcdh19* is expressed in cortical projection neurons that project through the corpus callosum (layer II-III and some layer V neurons), as well as in neurons projecting outside the cortex, mainly through the pyramidal tract (layer V PT neurons). Although several members of the cadherin superfamily, including delta protocadherins 7, 10, 17 and 18, have been shown to play a role in axonal outgrowth (Uemura et al., 2007; Piper et al., 2008; Hayashi et al., 2014), fasciculation (Williams et al., 2011; Hayashi et al., 2014) and arborization (Biswas et al., 2014), it is not known whether mutations in *Pcdh19* have an impact on any of these processes. We therefore conducted a general characterization of axonal tracts in Taconic *Pcdh19* male and female WT, male KO and female HET animals by immunostaining against the cell adhesion molecule L1CAM (Fig. 5A). No differences were apparent for males or females between genotypes in the major axonal tracts, including the internal capsule, stria terminalis, fimbria or corpus callosum. Next, we analyzed the corpus callosum in more detail by labelling dorsally located axons with Neuropilin-1, which allows the analysis of topographical organization at the midline. Again, the dorso-ventral extension of the corpus callosum and the dorsal restriction of Neuropilin-1 expressing axons was similar between genotypes for both male and female animals (Fig. 5B-D; Table 4[a,b]). Thus, our results revealed no major abnormalities in the main axonal tracts, although they do not preclude the existence of more subtle defects that would require a more detailed analysis to be revealed.

Altered behavior in *Pcdh19* mutant animals and their littermates

While there are no major lamination defects in the cortex and in the main axonal tracts of the brain of *Pcdh19* mutant animals, the changes in the distribution of specific neuronal subtypes revealed by our quantitative analysis could lead to local connectivity defects that could become apparent at the behavioral level. Indeed, synaptic defects have recently been described between *Pcdh19* WT and KO neurons (Mincheva-Tasheva et al., 2021; Hoshina et al., 2021). Thus, we also carried out a series of tests to determine whether these animals

present any behavioral alterations. The paradigms included open field to evaluate general locomotor activity, anxiety and exploratory behavior, elevated plus maze to measure anxiety, and a social interaction test. We assessed animals at preweaning age and as adults, to account for any developmental effects. In addition to the WT littermates that *Pcdh19* mutant animals were housed with, we included a further control of single genotype housed WT animals (WT^{SGH}) (Fig. 6A). Indeed, we note that a previous study on the X-linked ASD-related gene *Nlgn3*, also a membrane protein expressed in the developing cerebral cortex, revealed that housing conditions impact the behavior of wild-type animals when housed together with mutant animals (Kalbassi et al., 2017). The parents of the animals used to analyze behavior in the single genotype housed WT condition originated from our *Pcdh19* colony and behavior was analyzed separately for male and female mice. For the behavioral analysis we have added estimation statistics with confidence intervals (CIs) to the more common statistical inference analysis (one way ANOVA or Kruskal-Wallis test between the three groups) to improve the interpretation of results. Because estimation statistics compare the means of only two groups, we provide the average mean difference (*Mdiff*) and unbiased Cohen's *d* of the particular comparison with their corresponding 95% confidence intervals, followed by the results of the overall comparison with ANOVA or Kruskal-Wallis and the relevant post-hoc analysis. When the means of the three groups were not deemed different by any of the two methods, we only present the common statistical inference analysis for brevity.

Differences in male behavior were evident at P21 (Fig. 6B-E; Table 5). Mixed genotype housed WT males (WT^{MGH}) travelled on average 23% more distance during the 20 min open field paradigm than single genotype housed WT males (WT^{SGH}). The unpaired mean difference (M_{diff}) was 667.54 cm (95% CI[233.04, 1150.34], Fig. 6B) and the unbiased Cohen's *d* for this comparison was 0.89 (95% CI[0.29, 1.59]), indicating a strong effect of housing (one way ANOVA, $F(2,72) = 5.02$, $P = 0.0091$; post-hoc Tukey: $q(1,72) = 4.48$, $P = 0.0063$ WT^{MGH} vs WT^{SGH}). In this experiment, KO animals also travelled a higher distance than WT^{SGH} (M_{diff} = 281.06 cm, 95% CI[-25.36, 576.08]), but an effect of genotype cannot be

586 confirmed with these data. An analysis by 5-minute slots showed that the increased distance
587 travelled by WT^{MGH} males compared to WT^{SGH} males was mainly due to a 47% increase in
588 activity during the first 5 minutes (M_{diff} = 285.95 cm, 95% CI[112.15, 510.92]; unbiased
589 Cohen's *d* = 0.94 (95% CI [0.34, 1.65]; Kruskal-Wallis, *H*(2) = 9.35, *P* = 0.0093; post-hoc
590 Dunn: *Z* = 3.01, *P* = 0.0079 WT^{MGH} vs WT^{SGH}; Fig. 6C). Although KO males showed a 21%
591 increase in activity during this period when compared to WT^{SGH} males (M_{diff} = 127.75 cm,
592 95% CI[-4.02, 243.94]; unbiased Cohen's *d* = 0.53 (95% CI [0, 1.09]), this difference again
593 doesn't seem to reflect a real change in behavior, suggesting that increased activity might be
594 an effect of housing in males, rather than genotype (Kruskal-Wallis, *H*(2) = 9.35, *P* = 0.0093;
595 post-hoc Dunn: *Z* = 3.01, *P* = 0.1711 KO vs WT^{SGH}; Fig. 6C). The increased activity of
596 WT^{MGH} males over WT^{SGH} males disappeared after the first 5 minutes and also when
597 animals were tested again at ≥ P60 (Total distance M_{diff} = 351.78 cm, 95% CI[-197.54,
598 934.76]; unbiased Cohen's *d* = 0.36 (95% CI [-0.26, 1.02]; one way ANOVA, *F*(2,68) = 1.13,
599 *P* = 0.329; First 5 minutes: M_{diff} = 84.50 cm, 95% CI[-96.61, 256.31]; unbiased Cohen's *d* =
600 0.27 (95% CI [-0.35, 0.92]; one way ANOVA, *F*(2,68) = 1.31, *P* = 0.2759, Fig. 6-1A-C). In
601 accordance with these results, spontaneous activity (number of beam breaks) over a 24 h
602 period in adult male mice did not differ significantly between conditions (Fig. 6-1F,G), neither
603 when analyzed in total (one way ANOVA, *F*(2,34) = 0.48, *P* = 0.621), nor in the light (one
604 way ANOVA, *F*(2,34) = 3.03, *P* = 0.0615) or in the dark period (one way ANOVA, *F*(2,34) =
605 0.31, *P* = 0.733). Isolated differences at individual timepoints (19:00, Kruskal-Wallis, *H*(2) =
606 16.08, *P* = 0.0003; post-hoc Dunn: *Z* = 4.01, *P* = 0.0002 KO vs WT^{MGH}; 20:00, one way
607 ANOVA, *F*(2,34) = 5.18, *P* = 0.0109; post hoc Tukey: *q*(1,34) = 4.42, *P* = 0.0099 HET vs KO
608 vs WT^{SGH}; 10:00, Kruskal-Wallis, *H*(2) = 10.78, *P* = 0.0046; post-hoc Dunn: *Z* = 3.11, *P* =
609 0.0056 KO vs WT^{MGH}; *Z* = 2.62, *P* = 0.0267 KO vs WT^{SGH}; 8:00, Kruskal-Wallis, *H*(2) = 7.17,
610 *P* = 0.0277; post-hoc Dunn: *Z* = 2.51, *P* = 0.0361 WT^{MGH} vs KO; Fig. 6-1G) do not seem to
611 point to an overall activity defect and might be due to a smaller number of animals being
612 tested.

To investigate whether the increased distance travelled by pre-weaned mixed genotype housed WT animals in the first 5 minutes of the open field could be due to increased anxiety, we analyzed the time spent in the center of the arena. No differences were found between the three conditions, neither at P21 (Kruskal-Wallis, $H(2) = 2.76$, $P = 0.2518$), nor at P60 (Kruskal-Wallis, $H(2) = 3.58$, $P = 0.1671$, Fig. 6-1D). The results of the elevated plus maze confirmed the lack of differences at P21 (Kruskal-Wallis, $H(2) = 4.57$, $P = 0.1016$, Fig. 6-1E). However, this was not the case for adult animals, as adult KO males spent over 40% more time in the open arms than their WT^{MGH} littermates and WT^{SGH} controls, pointing to an effect of genotype in reducing anxiety (KO vs WT^{MGH}: $M_{diff} = 37.21$ sec, 95% CI[8.57, 59.45]; unbiased Cohen's $d = 0.80$ (95% CI [0.21, 1.46]; KO vs WT^{SGH}: $M_{diff} = 39.07$ sec, 95% CI[16.96, 61.53]; unbiased Cohen's $d = 0.90$ (95% CI [0.35, 1.52]; one way ANOVA, $F(2,68) = 6.88$, $P = 0.0019$; Tukey: $q(1,68) = 4.10$, $P = 0.0138$ KO vs WT^{MGH} and $q(1,68) = 4.68$, $P = 0.0042$ KO vs WT^{SGH}; Fig. 6D).

Interestingly, we also detected a subtle difference in social behavior at P21. In this case, WT^{MGH} males spent 19% less time interacting with an unfamiliar female in estrous than single-genotype housed WT males ($M_{diff} = -19.26$ sec, 95% CI[-33.73, -3.32]; unbiased Cohen's $d = -0.70$ (95% CI [-1.38, -0.10]; one way ANOVA, $F(2,72) = 3.39$, $P = 0.039$, Dunnett: $q(1,72) = 2.37$, $P = 0.0382$ WT^{MGH} vs WT^{SGH} Fig. 6E). Although KO males also showed a trend towards reduced interaction, with a 14% decrease ($M_{diff} = -14.59$ sec, 95% CI[-28.54, 0.18]; unbiased Cohen's $d = -0.52$ (95% CI [-1.08, 0.00]), this difference is even smaller than for WT^{MGH} males and unlikely to reflect a real change in behavior (Dunnett: $q(1,72) = 2.07$, $P = 0.0771$ HET vs WT^{SGH}). This result again points to an effect of housing on the social behavior of WT^{MGH} males.

In summary, adult KO males displayed a robust phenotype of reduced anxiety in the elevated plus maze test, and WT^{MGH} males showed altered behavior at P21, with increased activity during the first 5 minutes of the open field and reduced social interaction.

Changes in behavior were more pronounced in female mice than in their male counterparts (Table 6). We found again differences in the total distance travelled during the open field test at P21, with HET and WT^{MGH} females displaying an increase of 35% and 19%, respectively, when compared with single-genotype housed controls (HET vs WT^{SGH}: M_{diff} = 913.74 cm, 95% CI[494.07, 1314.30]; unbiased Cohen's d = 1.29 (95% CI [0.68, 2.04]; WT^{MGH} vs WT^{SGH}: M_{diff} = 486.76 cm, 95% CI[108.12, 853.27]; unbiased Cohen's d = 0.69 (95% CI [0.14, 1.31]; one way ANOVA, $F(2,69) = 9.54$, $P = 0.0002$, Tukey: $q(1,69) = 6.17$, $P = 0.0001$ for HET vs WT^{SGH} and $q(1,69) = 3.55$, $P = 0.0382$ for WT^{MGH} vs WT^{SGH}; Fig. 7A). Unlike in males, this effect was maintained at P60, but only in HET females, which travelled on average 19% more distance than WT^{SGH} animals (M_{diff} = 682.77 cm, 95% CI[189.66, 1149.25]; unbiased Cohen's d = 0.83 (95% CI [0.23, 1.51]; one way ANOVA, $F(2,69) = 3.99$, $P = 0.0229$; Tukey: $q(1,69) = 3.87$, $P = 0.0214$ for HET vs WT^{SGH}, Fig. 7B).

Analysis by 5-minute intervals showed that the increase in total distance was mainly due to increased activity during the first 5 minutes in the open field arena both at preweaning age and in adults (Fig. 7C,D). This effect was strong at both ages for HET females and their WT siblings when compared with single-genotype housed females, with increases of 95% (HET) and 54% (WT^{MGH}) at P21, and 53% (HET) and 49% (WT^{MGH}) in adult animals. At P21 the mean difference between HET and WT^{SGH} was M_{diff} = 388.61 cm, 95% CI[195.54, 576.41] with an unbiased Cohen's d = 1.49 (95% CI [0.87, 2.27]. Between WT^{MGH} and WT^{SGH}, M_{diff} = 289.11 cm, 95% CI[94.48, 465.99] with an unbiased Cohen's d = 0.96 (95% CI [0.40, 1.61] (Kruskal-Wallis, $H(2) = 21.86$, $P < 0.0001$; Dunn: $Z = 4.61$, $P < 0.0001$ HET vs WT^{SGH} and $Z = 3.12$, $P = 0.0055$ WT^{MGH} vs WT^{SGH} (Fig. 7C). Despite smaller percentage increases, the mean differences between HET and WT^{SGH}, and WT^{MGH} and WT^{SGH} at P60 rose to M_{diff} = 456.75 cm, 95% CI[304.66, 609.57] and M_{diff} = 426.36 cm, 95% CI[271.11, 595.22], respectively. The unbiased Cohen's d for those comparisons were d = 1.73 (95% CI [1.09, 2.55] and d = 1.39 (95% CI [0.82, 2.09]) (one way ANOVA, $F(2,69) = 17.95$, $P < 0.0001$, Tukey: $q(1,69) = 7.38$, $P < 0.0001$ HET vs WT^{SGH} and $q(1,69) = 7.43$, $P < 0.0001$ for WT^{MGH} vs WT^{SGH}, Fig. 7D). HET females also travelled a 25% longer distance than WT^{SGH} females

668 during the second 5-minute interval at P21 (M_{diff} = 215.18 cm, 95% CI[20.06, 391.89];
669 unbiased Cohen's d = 0.85 (95% CI [0.25, 1.54]; one way ANOVA, $F(2,69) = 3.29$, P =
670 0.0432; Tukey: $q(1,69) = 3.58$, P = 0.0359 HET vs WT^{SGH}, Fig. 7E), suggesting a potential
671 effect of genotype in addition to the housing effect. By P60, though, there was no average
672 change between the distance run in the second 5 minutes by any of the groups (Fig. 7F) and
673 no other differences were apparent during the rest of the testing period (Fig. 7-1A,B).
674 Similarly to male mice, the spontaneous activity over 24 h, measured as the number of
675 beam breaks, was not altered for any of the three experimental groups in the light (one way
676 ANOVA, main effect of genotype $F(2,36) = 2.29$, P = 0.1159), dark (one way ANOVA, main
677 effect of genotype $F(2,36) = 1.10$, P = 0.3429) or total periods (one way ANOVA, main effect
678 of genotype $F(2,36) = 1.08$, P = 0.3512) (Fig. 7-1C,D). Again, isolated differences were
679 evident at two timepoints during the dark phase (22:00, one way ANOVA, main effect of
680 genotype $F(2,36) = 3.84$, P = 0.0309, Tukey: $q(1,69) = 3.65$, P = 0.0364 WT^{MGH} vs WT^{SGH};
681 4:00, Welch's ANOVA $W(2, 23.61) = 8.52$, P = 0.0016, Dunnett T3: $t(2, 18.32) = 3.83$, P =
682 0.0036 WT^{MGH} vs HET; Dunnett T3: $t(2, 23.41) = 2.65$, P = 0.0417 WT^{MHG} vs WT^{SGH}, Fig. 7-
683 1D), but no overall changes in activity were apparent in this test.
684 Since the increase in distance travelled during the first 5 minutes in the open field test does
685 not seem to be caused by overall hyperactivity of HET animals and their WT siblings, we
686 again analyzed anxiety-related behaviors in these animals. There were no differences in the
687 time spent in the center of the open field arena for any of the conditions at P21 (Kruskal-
688 Wallis, $H(2) = 4.68$, P = 0.0962) or P60 (Kruskal-Wallis, $H(2) = 4.09$, P = 0.1296; Fig. 7-
689 1E,F), but, similar to the results obtained with male animals, HET females spent
690 considerably more time in the open arms of the elevated plus maze than any of the WT
691 females at P21 and P60 (Fig. 8A,B). The increases against WT^{SGH} and WT^{MGH} amounted to
692 76% and 103% at preweaning age (HET vs WT^{SGH}: M_{diff} = 50.69 sec, 95% CI[28.24, 78.00];
693 unbiased Cohen's d = 1.20 (95% CI [0.59, 1.94]; HET vs WT^{MGH}: M_{diff} = 59.71 sec, 95%
694 CI[34.28, 84.71]; unbiased Cohen's d = 1.32 (95% CI [0.74, 2.02]; Kruskal-Wallis, $H(2)$ =
695 20.94, $P < 0.0001$; Dunn: $Z = 3.19$, P = 0.042 between HET and WT^{SGH} and $Z = 4.49$, $P <$

696 0.0001 between WT^{MGH} and WT^{SGH}). In adults, the increase was down to 60% and 39%
697 (HET vs WT^{SGH}: M_{diff} = 42.40 sec, 95% CI[15.09, 69.81]; unbiased Cohen's d = 0.90 (95% CI
698 [0.30, 1.60]; HET vs WT^{MGH}: M_{diff} = 31.69 sec, 95% CI[7.28, 59.92]; unbiased Cohen's d =
699 0.71 (95% CI [0.15, 1.34]; one way ANOVA, $F(2,69) = 5.95$, $P = 0.0041$; Tukey: $q(1,69) =$
700 4.67, $P = 0.0043$ for HET vs WT^{SGH} and $q(1,69) = 3.72$, $P = 0.0281$ between HET and
701 WT^{MGH}). These results indicate a strong effect of genotype on reducing anxiety, as seen also
702 for adult male KO animals.
703 As in the case of male mice, the social interaction test revealed differences between single
704 and mixed genotype housed WT females (Fig. 8C,D). However, this effect was only present
705 in adult animals, with WT^{MGH} females spending 15% less time interacting with an unfamiliar
706 female in estrous (M_{diff} = -14.69 sec, 95% CI[-27.79, -1.29]; unbiased Cohen's d = -0.62
707 (95% CI [-1.24, -0.07]; one way ANOVA, $F(2,69) = 3.38$, $P = 0.0398$; Dunnett: $q(1,69) =$
708 2.32, $P = 0.0432$ WT^{MHG} vs WT^{SGH}).
709 Overall, we found significant behavioral differences between wild type and mutant animals
710 that were generally more pronounced in HET females than in KO males. HET females
711 displayed consistent hyperactivity during the first 5 minutes of the open field and, similar to
712 the mutant males, a robust phenotype of decreased anxiety in the elevated plus maze, in
713 this case both at preweaning and at adult stages. Importantly, we also uncovered an effect
714 of housing on the behavior of WT animals, with WT^{MGH} males and females presenting
715 significant differences in the open field and social interaction tests when compared to single
716 genotype housed WT animals.
717
718
719 **DISCUSSION**
720 Recent studies have shed light on the different functions of PCDH19 (Pederick et al., 2016;
721 Hayashi et al., 2017; Pham et al., 2017; Bassani et al., 2018; Homan et al., 2018; Pederick
722 et al., 2018; Serratto et al., 2020; Mincheva-Tasheva et al., 2021; Hoshina et al., 2021),
723 reviewed in (Gerosa et al., 2019; Gécz and Thomas, 2020), but we still have limited

724 knowledge about the neuronal types expressing PCDH19 and the consequences of *Pcdh19*
725 mutations on fine cortical composition, despite the relevance of these factors to understand
726 the pathological mechanisms underpinning EIEE9. Here we present a detailed analysis of
727 neuronal subtypes expressing *Pcdh19* in the mouse somatosensory cortex and a
728 comparison with human data. Our study reveals that *Pcdh19/PCDH19* is not only expressed
729 in pyramidal neurons, but also in different types of interneurons, and that, in general, higher
730 expression is limited to specific subpopulations in both cases. Our analysis also rules out
731 major anomalies in the main axonal tracts and provides a quantitative assessment of cortical
732 composition and lamination. Despite the lack of major architectural defects, our data reveal
733 subtle defects in layer composition that could contribute to the pathophysiology of EIEE9.
734 Indeed, mutant animals display behavioral alterations in the open field (females) and
735 elevated plus maze tests (males and females). Importantly, and as previously revealed with
736 the analysis of *Nlgn3* mutants (Kalbassi et al., 2017), the *Pcdh19* mutation affects the
737 behavior of wild-type littermates when housed in the same cage.
738
739 Hitherto, the characterization of the neuronal populations expressing PCDH19 has been
740 hindered by the lack of specific antibodies that perform satisfactorily in
741 immunohistochemistry analyses. In addition, as PCDH19 is likely distributed in both axons
742 and dendrites (Pederick et al., 2016; Hayashi et al., 2017; Bassani et al., 2018), the
743 unambiguous identification of cell bodies expressing PCDH19 is a challenging objective, as
744 is the case for most membrane proteins in the cortex. To overcome this difficulty, we
745 focused on the expression of *Pcdh19* mRNA, which is detected in the cell soma and allows a
746 better assessment of co-expression with other neuronal markers, which tend to be either
747 nuclear or cytoplasmic. Although mRNA and protein expression are not necessarily
748 correlated, available data show a good match between the regions with strongest mRNA
749 and protein signals (Hayashi et al., 2017; Pederick et al., 2018). Our ISH/IHC combination
750 approach provides experimental evidence for the expression of *Pcdh19* by different neuronal
751 types across cortical layers, including interneurons. We chose the somatosensory cortex to

carry out the analysis because it is a very well characterized area with a good definition of cortical layers. We then confirmed the results obtained in the postnatal SSC by choosing scRNAseq datasets that include neurons from various cortical regions (including SSC) from adult brain, which allowed us to obtain a global view of *Pcdh19/PCDH19* expression across cortical areas in mouse and human.

Our analysis of a mouse dataset of whole cortex and hippocampus confirmed that *Pcdh19* is expressed by excitatory neurons in Layer V, projecting both intra- and extra-cortically, as well as by certain subtypes of Layer II/III projection neurons, in agreement with the ISH data. Expression in layer IV is harder to judge from the scRNAseq results, as there are no clusters representing neurons from layer IV exclusively, but several clusters in layers VI and VIb also show high *Pcdh19* expression. In interneurons, expression is widespread in the Pvalb subclass, cluster specific in the Sncg, Vip, and Sst subclasses, and very low in the Lamp5 and Pax6 clusters, except for Lamp5 Lhx6, which shows high expression. These results demonstrate that while *Pcdh19* is expressed by a variety of excitatory and inhibitory neurons, expression remains specific for particular clusters. This cluster specificity would suggest a role for PCDH19 in the establishment of neuronal circuits as a potential neuronal recognition molecule.

Human *PCDH19* follows a similar pattern, with expression in both excitatory and inhibitory neuronal types. Expression in human excitatory neurons of the SSC is more graded, with many more subtypes showing intermediate expression levels than in mouse, likely reflecting an averaging effect due to the smaller number of human clusters defined for that dataset. In any case, highest expression corresponds to clusters in layers III and V, in line with RNA ISH results in mice. Regarding interneurons, high *PCDH19* expression can be found in subtypes of LAMP5, VIP, SST and PVALB interneurons, which generally show a good correlation with their murine counterparts. This is a relevant finding that supports the use of mouse models to investigate some aspects of *PCDH19* GCE. However, it is important to note that there are some differences as well, like the comparatively lower expression of *PCDH19* in long range projecting interneurons in humans (Inh L6 SST NPY in human,

780 Sst_Chodl in mouse). The functional relevance of *Pcdh19*/*PCDH19* expression in particular
781 neuronal subtypes will need to be established experimentally, but our results provide a
782 framework to support those functional studies in the future, not least because of regional
783 differences in the expression of this gene within neuronal subtypes.
784
785 To date, no detailed quantitative characterization of cortical composition and lamination has
786 been performed in the three existing *Pcdh19* KO models (Pederick et al., 2016; Hayashi et
787 al., 2017; Hoshina et al., 2021). We have quantified 5 excitatory and 4 inhibitory markers,
788 looking at overall abundance, as well as distribution throughout the cortical plate in the
789 somatosensory cortex. Our analysis, which was carried out separately in males and females,
790 reveals no differences in the abundance of the different excitatory neuronal types analyzed,
791 but points to small decreases in somatostatin expressing interneurons in HET females and
792 calretinin positive cells in KO males. We confirm the lack of major lamination defects
793 (Pederick et al., 2016; Hayashi et al., 2017; Hoshina et al., 2021); however, our quantitative
794 approach exposes more subtle changes in the distribution of certain neuronal types,
795 indicating altered composition of specific layers or sublayers. Although some changes might
796 represent false positives, such as the ones for HET Pvalb bin 8 and KO CR bin 7, which
797 might be explained by abnormal distributions that were apparent in the comparison between
798 WT males and females, it is worth noting that changes between genotypes were more
799 frequent and, in many cases, more significant, than between WT animals of opposite sex.
800 Indeed, we didn't find a single difference between WT males and females at P10, suggesting
801 that, although subtle, changes in layer composition cannot be ruled out in *Pcdh19* mutants.
802 Given the degree of neuronal diversity revealed by recent scRNAseq studies, our results
803 also support the possibility of more widespread differences affecting other neuronal
804 subtypes not covered by the antibodies used in our analysis. The origin of these differences
805 is unknown, but one possibility is that they could arise as a consequence of altered
806 neurogenesis, since PCDH19 has been shown to play a role in this process (Fujitani et al.,
807 2017; Homan et al., 2018; Lv et al., 2019). It is also important to consider that we carried out

808 our analysis mainly in the SSC, but given that *Pcdh19* expression varies between cortical
809 regions, it is possible that different areas might be affected in different ways by a total or
810 partial loss of PCDH19. Reports of focal cortical dysplasia and limbic abnormalities in EIEE9
811 patients (Kurian et al., 2018; Pederick et al., 2018; Lenge et al., 2020) and focal areas of
812 disorganization in ASD patients (Stoner et al., 2014) seem to support this possibility.
813
814 Despite the involvement of other delta protocadherins in the development of axonal tracts
815 (Uemura et al., 2007; Piper et al., 2008; Biswas et al., 2014; Hayashi et al., 2014), our data
816 do not support a major role of PCDH19 in this process. We did not detect any alterations in
817 the main axonal tracts in the brain after staining for the axonal protein L1CAM, and a more
818 detailed analysis of the corpus callosum also showed no differences in its dorso-ventral
819 extension or the dorsal restriction of Neuropilin-1 expressing axons. This is in agreement
820 with the lack of defects found by Hayashi et al. in the projection of axons through this
821 particular tract (Hayashi et al., 2017). More subtle defects in specific tracts would require
822 much deeper analyses to be revealed, as the defects in cortical axonal arborization recently
823 described in *Pcdh19* HET animals (Mincheva-Tasheva et al., 2021).
824
825 Regardless of any anatomical alterations, investigating behavior allows a relevant functional
826 assessment of the consequences of *Pcdh19* loss. Our analysis differed from previous
827 studies (Hayashi et al., 2017; Lim et al., 2019) in two main ways: first, in addition to adult
828 animals, we also tested animals at a much younger age (pre-weaning, P21), as EIEE9 is a
829 developmental disorder and therefore it is relevant to determine when any behavioral
830 changes begin. Second, we added a second cohort of control animals: wild-type single
831 genotype housed mice, that have only been exposed to other WT animals during their life.
832 An effect of WT littermates on the behavior of mutant animals was shown by Yang et al
833 when they demonstrated that raising less sociable BTBR T+tf/J mice with highly sociable
834 C57Bl6/J animals improved BTBR T+tf/J sociability (Yang et al., 2011). However, the impact
835 of social environment on the behavior of WT littermates has only recently been

836 demonstrated in a study with mice mutant for *Nlgn3*, an X-linked cell adhesion protein that
837 has been implicated in ASD (Kalbassi et al., 2017). Therefore, this is further evidence to
838 suggest that mutant mice can alter the behavior of their WT littermates and to support the
839 addition of single genotype housed WT controls.
840
841 In line with a previous mouse study (Hayashi et al., 2017) and with the findings in human
842 patients, changes in behavior were more apparent in HET females than in their KO male
843 siblings. *Pcdh19* KO males only showed increased time spent in the open arms of the EPM,
844 indicating reduced anxiety, when tested as adults. This same behavior was displayed by
845 young *Pcdh19* HET females (P21), which maintained it into adulthood. However, HET
846 females also exhibited increased exploratory behavior, or maybe hypersensitivity to new
847 environments, from a young age, as demonstrated by their consistently higher distance
848 travelled during the first 5 minutes in the open field at P21 and P60. It is important to
849 consider that animals were placed into the open field arena 4 times in total, as they were
850 tested on two consecutive days at both ages. Although habituation to the environment would
851 be expected in this situation, the increased distance travelled during the first 5 minutes was
852 apparent in all 4 trials, indicating a robust behavioral response. These results also suggest
853 that behavioral changes in *Pcdh19* heterozygous animals start early in life, validating them
854 as a good model for a developmental condition.
855 Open field and EPM tests were also performed in the study by Hayashi et al (Hayashi et al.,
856 2017). They found no differences in the EPM, but this could be due to differences in
857 experimental design or in the mouse model used for the test. Regarding the open field test,
858 Hayashi et al found no differences in total distance or time in the center when the test was
859 conducted at 11-12 weeks of age. However, when they repeated the test 23 weeks later,
860 *Pcdh19* HET females spent significantly more time in the center of the open field arena,
861 suggesting reduced anxiety. Although our animals did not display such behavior, they were
862 tested around P60, which would be in agreement with the data from their first open field test.
863 In addition, the results of our EPM test also indicate reduced anxiety in our animals, which

could therefore represent a behavioral characteristic of *Pcdh19* mutant animals. Because no specific analysis of the first 5 minutes was carried out in that study, it is difficult to assess whether their animals exhibited increased activity during that period. Nevertheless, the fact that WT females display the same behavioral phenotype as their HET siblings indicates an effect of the social environment that can only be detected through the inclusion of single genotype housed WT animals. Interestingly, this effect was also present in young males, with WT^{MGH} travelling a higher distance in the first 5 minutes of the open field test than KO or WT^{SGH} males. However, unlike in the female population, this behavior disappeared in adulthood. Because adult male and female animals are housed separately, it is tempting to speculate that this effect of the social environment is somehow mediated by the HET females, although other causes, like a maternal effect, cannot be ruled out based on our experiments.

One of the comorbidities of EIEE9 patients is ASD (Kolc et al., 2020), and changes in *PCDH19* have also been linked to ASD cases (Piton et al., 2010; Harssel et al., 2013). Indeed, a recent behavioral study with the Taconic *Pcdh19* KO mouse model has revealed social interaction deficits in the three chamber test in KO males and HET females, as well as increased repetitive behavior in males (females were not tested) (Lim et al., 2019). In our analysis, we also found differences in social behavior, but, interestingly, only in WT^{MGH} animals. Both males and females spent less time interacting with a stranger female at P21 and P60, respectively, than WT^{SGH} animals, in what appears to be another example of the effect of the environment on mouse behavior. Since males were not tested at P60, because at that age it becomes a measure of courtship behavior rather than simple social interaction and as such is not comparable to the P21 behavior, we don't know if this phenotype would be maintained into adulthood or if, similar to the results of the open field, it would revert to normal with age. The fact that HET and KO animals did not differ in their behavior from their WT littermates is in contradiction with the results from Lim et al, although different tests were carried out in both studies, making a direct comparison difficult. In summary, our behavioral characterization of the *Pcdh19* Taconic mouse model reveals a stronger effect of *Pcdh19*

892 mutation in HET females than in KO males and a significant effect of the social environment
893 on the behavior of WT littermates, as previously described for *Nlgn3* mutant animals
894 (Kalbassi et al., 2017). This is a relevant finding, and this effect should be taken into
895 consideration for the design of future behavioral experiments, as failure to do so could result
896 in misinterpretation of data and missed behavioral phenotypes. It is important to note that,
897 despite the subtle differences found in cortical composition in the SSC, we believe that a
898 correlation between those changes and the observed behavioral alterations cannot be made
899 at this point. Different cortical and brain regions are involved in the control of the behavioral
900 paradigms that we have analyzed, so isolated cellular results of one cortical area, however
901 widespread they might be, cannot be linked to any specific aspects of behavior. Such a
902 correlation would require functional assays of neuronal function to go beyond mere
903 speculation.
904
905 Finally, an important question is why mutation of *Pcdh19* in mice leads to much milder
906 defects than in humans, with the absence of seizures as the most striking difference. It is
907 worth noting that similar results have been described for other neurodevelopmental
908 disorders that present with epilepsy, such as CDKL5 Deficiency Disorder (CDD) or Fragile X
909 Syndrome (FXS). Mice carrying either a null allele for *Cdkl5* or the disease-causing mutation
910 R59X do not display behavioral seizures, but they exhibit network hyper-excitability that
911 manifests as decreased threshold to pharmacologically induced seizures (Wang et al., 2012;
912 Amendola et al., 2014). In the case of FXS, in which about 20% of patients develop epilepsy
913 (Musumeci et al., 1999; Sabaratnam et al., 2001), none of the KO mouse models presents
914 spontaneous seizures. However, they are susceptible to audiogenic seizures and display
915 alterations in cortical EEG frequency (Musumeci et al., 2000; Lovelace et al., 2018;
916 Goswami et al., 2019). Similarly, cortical network activity is altered in *Pcdh19* heterozygous
917 animals (Pederick et al., 2018), indicating that mutations in those genes in mice do alter
918 cortical connectivity, but not enough to trigger seizures. The smaller size and reduced
919 complexity of the mouse brain probably account, at least partially, for these discrepancies,

maybe by conferring a generally lower susceptibility to seizures in mice. Therefore, considering recent progress in the use of brain organoids for the study of neuronal connectivity (Quadrato et al., 2017), this emerging model might be needed in the future to dissect the effects of *PCDH19* mutations on human connectivity.

REFERENCES

Amendola E, Zhan Y, Mattucci C, Castroflorio E, Calcagno E, Fuchs C, Lonetti G, Silingardi D, Vyssotski AL, Farley D, Ciani E, Pizzorusso T, Giustetto M, Gross CT (2014) Mapping Pathological Phenotypes in a Mouse Model of CDKL5 Disorder D'Esposito M, ed. PLoS ONE 9:e91613.

Bassani S, Cwetsch AW, Gerosa L, Serratto GM, Folci A, Hall IF, Mazzanti M, Cancedda L, Passafaro M (2018) The female epilepsy protein PCDH19 is a new GABAAR binding partner that regulates GABAergic transmission as well as migration and morphological maturation of hippocampal neurons. Hum Mol Genet 27:1027–1038.

Biswas S, Emond MR, Duy PQ, Hao LT, Beattie CE, Jontes JD (2014) Protocadherin-18b interacts with Nap1 to control motor axon growth and arborization in zebrafish. Mol Biol Cell 25:633–642.

Caligioni CS (2009) Assessing reproductive status/stages in mice. Curr Protoc Neurosci Appendix 4:Appendix4I–A.4I.8.

Chen B, Brinkmann K, Chen Z, Pak CW, Liao Y, Shi S, Henry L, Grishin NV, Bogdan S, Rosen MK (2014) The WAVE regulatory complex links diverse receptors to the actin cytoskeleton. Cell 156:195–207.

943 Cooper SR, Emond MR, Duy PQ, Liebau BG, Wolman MA, Jontes JD (2015)
944 Protocadherins control the modular assembly of neuronal columns in the zebrafish optic
945 tectum. J Cell Biol 211:807–814.

946 Depienne C et al. (2009) Sporadic infantile epileptic encephalopathy caused by mutations in
947 PCDH19 resembles Dravet syndrome but mainly affects females. Meisler MH, ed. PLoS
948 Genet 5:e1000381.

949 Depienne C, Leguern E (2012) PCDH19-related infantile epileptic encephalopathy: An
950 unusual X-linked inheritance disorder Rosenblatt DS, Majewski J, eds. Human Mutation
951 33:627–634.

952 Dibbens LM et al. (2008) X-linked protocadherin 19 mutations cause female-limited epilepsy
953 and cognitive impairment. Nat Genet 40:776–781.

954 Duszyc K, Terczynska I, Hoffman-Zacharska D (2015) Epilepsy and mental retardation
955 restricted to females: X-linked epileptic infantile encephalopathy of unusual inheritance.
956 J Appl Genet 56:49–56.

957 Emond MR, Biswas S, Jontes JD (2009) Protocadherin-19 is essential for early steps in
958 brain morphogenesis. Dev Biol 334:72–83.

959 Fujitani M, Zhang S, Fujiki R, Fujihara Y, Yamashita T (2017) A chromosome 16p13.11
960 microduplication causes hyperactivity through dysregulation of miR-484/protocadherin-
961 19 signaling. Mol Psychiatry 22:364–374.

962 Gaitan Y, Bouchard M (2006) Expression of the δ-protocadherin gene Pcdh19 in the
963 developing mouse embryo. Gene Expression Patterns 6:893–899.

964 Gerosa L, Francolini M, Bassani S, Passafaro M (2019) The Role of Protocadherin 19
965 (PCDH19) in Neurodevelopment and in the Pathophysiology of Early Infantile Epileptic
966 Encephalopathy-9 (EIEE9) Hsueh YP, Xiong Z-Q, eds. Dev Neurobiol 79:75–84.

967 Gécz J, Thomas PQ (2020) Disentangling the paradox of the PCDH19 clustering epilepsy, a
968 disorder of cellular mosaics. Curr Opin Genet Dev 65:169–175.

969 Goswami S, Cavalier S, Sridhar V, Huber KM, Gibson JR (2019) Local cortical circuit
970 correlates of altered EEG in the mouse model of Fragile X syndrome. Neurobiol Dis
971 124:563–572.

972 Harssel JJT et al. (2013) Clinical and genetic aspects of PCDH19-related epilepsy
973 syndromes and the possible role of PCDH19 mutations in males with autism spectrum
974 disorders. Neurogenetics 14:23–34.

975 Hayashi S, Inoue Y, Hattori S, Kaneko M, Shioi G, Miyakawa T, Takeichi M (2017) Loss of
976 X-linked Protocadherin-19 differentially affects the behavior of heterozygous female and
977 hemizygous male mice. Sci Rep 7:5801.

978 Hayashi S, Inoue Y, Kiyonari H, Abe T, Misaki K, Moriguchi H, Tanaka Y, Takeichi M (2014)
979 Protocadherin-17 Mediates Collective Axon Extension by Recruiting Actin Regulator
980 Complexes to Interaxonal Contacts. Dev Cell.

981 Hertel N, Redies C (2010) Absence of Layer-Specific Cadherin Expression Profiles in the
982 Neocortex of the Reeler Mutant Mouse. Cereb Cortex.

983 Hodge RD et al. (2019) Conserved cell types with divergent features in human versus
984 mouse cortex. Nature 573:61–68.

985 Homan CC, Pederson S, To T-H, Tan C, Piltz S, Corbett MA, Wolvetang E, Thomas PQ,
986 Jolly LA, Gécz J (2018) PCDH19 regulation of neural progenitor cell differentiation
987 suggests asynchrony of neurogenesis as a mechanism contributing to PCDH19 Girls
988 Clustering Epilepsy. Neurobiol Dis 116:106–119.

989 Hoshina N, Johnson-Venkatesh EM, Hoshina M, Umemori H (2021) Female-specific
990 synaptic dysfunction and cognitive impairment in a mouse model of PCDH19 disorder.
991 Science 372:eaaz3893.

992 Kalbassi S, Bachmann SO, Cross E, Roberton VH, Baudouin SJ (2017) Male and Female
993 Mice Lacking Neuroligin-3 Modify the Behavior of Their Wild-Type Littermates. eNeuro
994 4:ENEURO.0145–17.2017.

995 Kolc KL, Sadleir LG, Depienne C, Marini C, Scheffer IE, Moller RS, Trivisano M, Specchio N,
996 Pham D, Kumar R, Roberts R, Gécz J (2020) A standardized patient-centered
997 characterization of the phenotypic spectrum of PCDH19 girls clustering epilepsy. Transl
998 Psychiatry 10:127.

999 Kolc KL, Sadleir LG, Scheffer IE, Ivancevic A, Roberts R, Pham DH, Gécz J (2018) A
1000 systematic review and meta-analysis of 271 PCDH19-variant individuals identifies
1001 psychiatric comorbidities, and association of seizure onset and disease severity. Mol
1002 Psychiatry 79:1.

1003 Kurian M, Korff CM, Ranza E, Bernasconi A, Lübbig A, Nangia S, Ramelli GP, Wohlrab G,
1004 Nordli DR, Bast T (2018) Focal cortical malformations in children with early infantile
1005 epilepsy and PCDH19 mutations: case report. Dev Med Child Neurol 60:100–105.

1006 Lake BB et al. (2016) Neuronal subtypes and diversity revealed by single-nucleus RNA
1007 sequencing of the human brain. Science 352:1586–1590.

1008 Lenge M, Marini C, Canale E, Napolitano A, De Masi S, Trivisano M, Mei D, Longo D, Rossi
1009 Espagnet MC, Lucenteforte E, PCDH19 Clinical Study Group, Barba C, Specchio N,
1010 Guerrini R (2020) Quantitative MRI-Based Analysis Identifies Developmental Limbic
1011 Abnormalities in PCDH19 Encephalopathy. Cereb Cortex 12:526.

1012 Lim J, Ryu J, Kang S, Noh HJ, Kim CH (2019) Autism-like behaviors in male mice with a
1013 Pcdh19 deletion. Molecular Brain 12:95.

1014 Lovelace JW, Ethell IM, Binder DK, Razak KA (2018) Translation-relevant EEG phenotypes
1015 in a mouse model of Fragile X Syndrome. Neurobiol Dis 115:39–48.

1016 Lv X, Ren S-Q, Zhang X-J, Shen Z, Ghosh T, Xianyu A, Gao P, Li Z, Lin S, Yu Y, Zhang Q,
1017 Groszer M, Shi S-H (2019) TBR2 coordinates neurogenesis expansion and precise
1018 microcircuit organization via Protocadherin 19 in the mammalian cortex. Nat Comms
1019 10:1–15.

1020 Mincheva-Tasheva S, Guil AFN, Homan CC, Gecz J, Thomas PQ (2021) Disrupted
1021 Excitatory Synaptic Contacts and Altered Neuronal Network Activity Underpins the
1022 Neurological Phenotype in PCDH19-Clustering Epilepsy (PCDH19-CE). Mol Neurobiol
1023 58:2005–2018.

1024 Musumeci SA, Bosco P, Calabrese G, Bakker C, De Sarro GB, Elia M, Ferri R, Ben A
1025 Oostra (2000) Audiogenic Seizures Susceptibility in Transgenic Mice with Fragile X
1026 Syndrome. Epilepsia 41:19–23.

1027 Musumeci SA, Hagerman RJ, Ferri R, Bosco P, Bernardina BD, Tassinari CA, De Sarro GB,
1028 Elia M (1999) Epilepsy and EEG Findings in Males with Fragile X Syndrome. Epilepsia
1029 40:1092–1099.

1030 Paul A, Crow M, Raudales R, He M, Gillis J, Huang ZJ (2017) Transcriptional Architecture of
1031 Synaptic Communication Delineates GABAergic Neuron Identity. Cell 171:522-539.e20.

1032 Pederick DT, Homan CC, Jaehne EJ, Piltz SG, Haines BP, Baune BT, Jolly LA, Hughes JN,
1033 Gécz J, Thomas PQ (2016) Pcdh19 Loss-of-Function Increases Neuronal Migration In
1034 Vitro but is Dispensable for Brain Development in Mice. Sci Rep 6:26765.

1035 Pederick DT, Richards KL, Piltz SG, Kumar R, Mincheva-Tasheva S, Mandelstam SA, Dale
1036 RC, Scheffer IE, Gécz J, Petrou S, Hughes JN, Thomas PQ (2018) Abnormal Cell
1037 Sorting Underlies the Unique X-Linked Inheritance of PCDH19 Epilepsy. Neuron 97:59–
1038 66.e5.

1039 Pham DH, Tan CC, Homan CC, Kolc KL, Corbett MA, McAninch D, Fox AH, Thomas PQ,
1040 Kumar R, Gécz J (2017) Protocadherin 19 (PCDH19) interacts with paraspeckle protein
1041 NONO to co-regulate gene expression with estrogen receptor alpha (ERα). Hum Mol
1042 Genet 26:2042–2052.

1043 Piper M, Dwivedy A, Leung L, Bradley RS, Holt CE (2008) NF-protocadherin and TAF1
1044 regulate retinal axon initiation and elongation in vivo. J Neurosci 28:100–105.

1045 Piton A et al. (2010) Systematic resequencing of X-chromosome synaptic genes in autism
1046 spectrum disorder and schizophrenia. Mol Psychiatry 16:867–880.

1047 Quadrato G, Nguyen T, Macosko EZ, Sherwood JL, Min Yang S, Berger DR, Maria N,
1048 Scholvin J, Goldman M, Kinney JP, Boyden ES, Lichtman JW, Williams ZM, McCarroll
1049 SA, Arlotta P (2017) Cell diversity and network dynamics in photosensitive human brain
1050 organoids. Nature 545:48–53.

1051 Sabaratnam M, Vroegop PG, Gangadharan SK (2001) Epilepsy and EEG findings in 18
1052 males with fragile X syndrome. Seizure 10:60–63.

1053 Schindelin J, Arganda-Carreras I, Frise E, Kaynig V, Longair M, Pietzsch T, Preibisch S,
1054 Rueden C, Saalfeld S, Schmid B, Tinevez J-Y, White DJ, Hartenstein V, Eliceiri K,
1055 Tomancak P, Cardona A (2012) Fiji: an open-source platform for biological-image
1056 analysis. Nat Meth 9:676–682.

1057 Serratto GM, Pizzi E, Murru L, Mazzoleni S, Pelucchi S, Marcello E, Mazzanti M, Passafaro
1058 M, Bassani S (2020) The Epilepsy-Related Protein PCDH19 Regulates Tonic Inhibition,

GABAAR Kinetics, and the Intrinsic Excitability of Hippocampal Neurons. Mol Neurobiol 57:5336–5351.

Stoner R, Chow ML, Boyle MP, Sunkin SM, Mouton PR, Roy S, Wynshaw-Boris A, Colamarino SA, Lein ES, Courchesne E (2014) Patches of disorganization in the neocortex of children with autism. N Engl J Med 370:1209–1219.

Tan C et al. (2015) Mutations of protocadherin 19 in female epilepsy (PCDH19-FE) lead to allopregnanolone deficiency. Hum Mol Genet 24:5250–5259.

Tasic B et al. (2018) Shared and distinct transcriptomic cell types across neocortical areas. Nature 563:72–78.

Terracciano A, Trivisano M, Cusmai R, De Palma L, Fusco L, Compagnucci C, Bertini E, Vigevano F, Specchio N (2016) PCDH19-related epilepsy in two mosaic male patients. Epilepsia 57:e51–e55.

Trivisano M, Lucchi C, Rustichelli C, Terracciano A, Cusmai R, Ubertini GM, Giannone G, Bertini ES, Vigevano F, Gécz J, Biagini G, Specchio N (2017) Reduced steroidogenesis in patients with PCDH19-female limited epilepsy. Epilepsia 13:35.

Uemura M, Nakao S, Suzuki ST, Takeichi M, Hirano S (2007) OL-protocadherin is essential for growth of striatal axons and thalamocortical projections. Nat Neurosci 10:1151–1159.

Wang I-TJ, Allen M, Goffin D, Zhu X, Fairless AH, Brodkin ES, Siegel SJ, Marsh ED, Blendy JA, Zhou Z (2012) Loss of CDKL5 disrupts kinome profile and event-related potentials leading to autistic-like phenotypes in mice. Proc Natl Acad Sci USA 109:21516–21521.

Williams EO, Sickles HM, Dooley AL, Palumbos S, Bisogni AJ, Lin DM (2011) Delta Protocadherin 10 is Regulated by Activity in the Mouse Main Olfactory System. Frontiers in Neural Circuits 5:9.

1082 Wolverton T, Lalande M (2001) Identification and characterization of three members of a
1083 novel subclass of protocadherins. Genomics 76:66–72.

1084 Yang M, Perry K, Weber MD, Katz AM, Crawley JN (2011) Social peers rescue autism-
1085 relevant sociability deficits in adolescent mice Crawley J, DiCicco-Bloom E, Bailey AJ,
1086 eds. Autism Res 4:17–27.

1087 Yao Z et al. (2020) A taxonomy of transcriptomic cell types across the isocortex and
1088 hippocampal formation. Biorxiv 2020.03.30.015214.

1089

1090

1091 **TABLE AND FIGURE LEGENDS**

1092

1093 **Table 1. Comparison of GABAergic clusters with high *Pcdh19* expression in mouse**
1094 **and human SSC.**
1095 GABAergic clusters with high *Pcdh19* expression in the SSC from either the mouse “Whole
1096 Cortex & Hippocampus - SMART-SEQ (2019) with 10X-Smart-Seq Taxonomy (2020)” or the
1097 human “Multiple Cortical Areas – SMART-SEQ (2019)” datasets are listed in the left and
1098 right columns of the table, respectively. The middle columns list the clusters and
1099 homologous cell type taxonomy groups that have allowed the indirect correlation between
1100 them. H, high expression; M, medium expression; L, low expression; N.P., cluster is not
1101 present in the SSC.

1102

1103 **Table 2. Statistical analysis of cortical width and marker composition at P10.**
1104 The table lists the data analyzed and the groups that have been compared, including the
1105 number of independent samples. Normality of the data and equality of variance for the
1106 groups compared are indicated, as well as the statistical test performed and the obtained

results. The details of the tests performed for the layer distribution of individual markers have not been included for simplicity.

Table 3. Statistical analysis of cortical width and marker composition at P20.
The table includes the data analyzed and the comparisons made, listing the number of independent samples. Normality of the data and equality of variance for the groups compared are included, as well as the statistical test performed and the obtained results. The details of the tests performed for the layer distribution of individual markers have not been included for simplicity.

Table 4. Statistical analysis of dorso-ventral extension and NRP1/L1CAM ratio in the corpus callosum of wild type and *Pcdh19* mutant pups.
The table lists the data analyzed and the groups that have been compared, including the number of independent samples. Normality of the data and equality of variance for the groups compared are indicated, as well as the statistical test performed and the obtained results.

Table 5. Statistical analysis of the behavioral experiments in P21 and adult males.
The table includes the behavioral test analyzed, sex and age of the animals, data and variance distribution, statistical test used, and results obtained.

Table 6. Statistical analysis of the behavioral experiments in P21 and adult females.
The table includes the behavioral test analyzed, sex and age of the animals, data and variance distribution, statistical test used, and results obtained.

Figure 1. *Pcdh19* is expressed by excitatory and inhibitory neurons in the mouse cortex.

(A-D) Confocal micrographs of P10 (A-C) and P20 (D) cortical slices hybridized with an RNA probe against *Pcdh19* (red) and antibodies against (A) RORB (green), (B) SATB2 and CTIP2 (green and blue, respectively), (C) TBR1 (green) and (D) Parvalbumin (Pvalb, green). The left panel shows the entire cortical wall with boxes indicating the regions enlarged in the right panels. White arrowheads point to double positive cells, empty arrowheads point to single positive cells (*Pcdh19* negative). Scale bars: left panels, 100 μm; right panels, 50 μm. (E) Strategy of the analysis of the Mouse whole cortex & hippocampus dataset. (F) Violin plots representing gene expression and distribution for *Pcdh19* and the markers used in (A-D) in the 15 subclasses that the SSC neurons analyzed belong to. Four extra subclasses with 5 or fewer cells are not included in the figure. (G,H) Violin plots representing gene expression and distribution for *Pcdh19* and the markers used in (A-D) in the different excitatory (G) and interneuronal (H) clusters defined in the Yao et al., 2020 study (Allen Brain Atlas Whole Cortex & Hippocampus - SMART-SEQ (2019) with 10X-Smart-Seq Taxonomy (2020). Dots indicate the median value of the cluster in CPM. CPM values are displayed on $\log_{10}$ scale. For simplicity, clusters belonging to the 4 subclasses not included in (F) and any cluster with less than 3 neurons are also not represented in this figure. Gene expression and distribution of *Pcdh19* in cortical excitatory and inhibitory neurons of the Allen Brain Atlas mouse Whole Cortex & Hippocampus dataset, both globally and by specific brain region, can be found in Extended Data Figure 1-1 and 1-2, respectively.

Figure 2. *PCDH19* is expressed by excitatory and inhibitory neurons in the human cortex.

(A) Strategy of the analysis of the Human – Multiple Cortical Areas SMART Seq dataset. (B) Violin plots representing gene expression and distribution for *Pcdh19* and the markers used in (A-D) in the 12 subclasses that the SSC neurons analyzed belong to. (C,D) Gene expression and distribution of *PCDH19* in the glutamatergic (C) and GABAergic (D) cell

clusters of the human SSC, represented by violin plots. For the excitatory clusters, the corresponding subclasses are indicated at the top. Dots indicate the median value of the cluster in CPM. CPM values are displayed on $\log_{10}$ scale. For simplicity any cluster with less than 3 neurons is not represented in this figure. Gene expression and distribution of *PCDH19* in cortical excitatory and inhibitory neurons of the Allen Brain Atlas human Multiple Cortical Areas dataset, both globally and by specific brain region, can be found in Extended Data Figure 2-1 and 2-2, respectively. For the strategy to indirectly correlate human and mouse clusters, the specific mouse and human neuronal GABAergic subtypes assigned to the different homology clusters and the correspondence between the nuclei from the MTG and the Multiple Cortical Areas datasets please see Extended Data Figure 2-3.

Figure 3. Subtle, but significant changes in the distribution of cortical excitatory neurons in *Pcdh19* mutant animals.

(A) Quantification of cortical width at P10 in *Pcdh19* WT and mutant animals, separated by sex. (B) Relative percentage of CUX1+ cells examined with respect to total DAPI+ cells in *Pcdh19* WT, HET and KO animals. (C) Relative percentages of the different cortical markers examined with respect to total DAPI+ cells. Analysis performed separately for males and females. (D) Representative confocal micrographs of immunohistochemistry with anti-CUX1 (red) and anti-CTIP2 (green) antibodies on WT male, KO male, WT female and HET female tissue. (E) Quantification of the percentage of CUX+ cells in each of 10 equal bins spanning the cortical wall. (F) Distribution of CTIP2+ cells in each of 10 equal bins spanning the cortical wall, shown as percentage, for males (left) and females (right). (G,I) Representative confocal micrographs of immunohistochemistry with anti-RORB (red) and anti-SATB2 (green) antibodies on WT and KO male tissue (G) and WT and HET female tissue (I). (H,J) Quantification of the percentage of RORB+ (left) and SATB2+ (right) cells in each of 10 equal bins spanning the cortical wall. (K) Representative confocal micrographs of immunohistochemistry with anti-TBR1 (red) antibodies on antibodies on WT male, KO male, WT female and HET female tissue. Nuclei are counterstained with DAPI (blue). (L)

Distribution of TBR1+ cells in each of 10 equal bins spanning the cortical wall, shown as percentage for males (left) and females (right). All results are indicated as mean ± SEM. A minimum of 3 images per brain, obtained from four animals originating from three different litters were analyzed for each condition. *P < 0.05; **P < 0.01. Scale bars: 200 μm.

Figure 4. Subtle changes in the distribution of inhibitory neurons in the cortex of *Pcdh19* mutant animals.

(A) Quantification of cortical width at P20 in *Pcdh19* WT and mutant animals, separated by sex. (B) Relative percentages of the different cortical markers examined with respect to total DAPI+ cells in the somatosensory cortex. Analysis performed separately for males and females. (C,E) Representative confocal micrographs of immunohistochemistry with anti-Calbindin (CB, red) and anti-Somatostatin (SST, green) antibodies on WT and KO male tissue (C), and WT and HET female tissue (right). Inserts: high magnification of SST+ cells. Nuclei were counterstained with DAPI (blue). (D,F) Quantification of the percentage of CB+ (left) and SST+ (right) cells in each of 10 equal bins spanning the cortical wall for males (D) and females (F). (G,I) Representative confocal micrographs of immunohistochemistry with anti-Parvalbumin (Pvalb, red) and anti-Calretinin (CR, green) antibodies on WT and KO male tissue (C), and WT and HET female tissue (right). (H,J) Distribution of CR+ (left) and Pvalb+ (right) cells in each of 10 equal bins spanning the cortical wall, shown as percentage. Male data shown in (H) and female data in (J). All results are indicated as mean ± SEM. A minimum of 3 images per brain, obtained from four animals originating from three different litters were analyzed for each condition. *P < 0.05, **P < 0.01. Scale bars: 200 μm; insets: 50 μm.

Figure 5. No major anomalies in the main axonal tracts in *Pcdh19* mouse mutants.

(A) Confocal micrographs of P0-P1 mouse hemispheres stained with anti-L1CAM (red). Nuclei were counterstained with DAPI (blue). (B) Confocal micrographs of the corpus callosum of P0-P1 mice stained with anti-L1CAM (red), anti-Neuropilin-1 (green) and

counterstained with DAPI (blue). (C) Quantification of the dorso-ventral extension of the corpus callosum in WT and mutant animals, separated by sex. (D) Quantification of the dorsal restriction of Neuropilin-1 positive axons in WT and mutant animals, separated by sex. All results are indicated as mean ± SEM. 2 images per brain, obtained from four animals originating from three different litters were analyzed for each condition. Cx, cortex; Hip, hippocampus; Th, thalamus, fi, fimbria; st, striatum; ic, internal capsule; Cg, cingulate cortex; cc, corpus callosum; hc, hippocampal commissure. Scale bars: 200 μm (A) and 50 μm (B).

Figure 6. Behavioral alterations in *Pcdh19* KO males and their WT littermates. (A) Schematic of the behavioral experiments carried out. (B) Total distance travelled by males during the 20 minutes of the open field test at P21. (C) Distance travelled in the open field by P21 males in the first 5-minute interval of the open field test. Open field results correspond to the second day of testing in (a) and (B). (D) Total time spent by males in the open arms of the elevated plus maze during the 5-minute test at P60. (E) Time spent by P21 males interacting with a non-familiar female in oestrus. The total duration of the test was 5 minutes. For panels B-D, the upper axis shows the raw data points for each group. To their right, the gap in the line indicates the mean, and the lines extending vertically represent the standard deviation. The group and group sizes are indicated at the bottom. Note that each group appears twice in every graph, but with two different colors. The mean difference for each comparison is plotted in the lower axis as a bootstrap sampling distribution. The black dot represents the mean and the vertical bar it's 95% confidence interval. At the top of each graph the significance scores of the one-way ANOVA or Kruskal-Wallis test and their post-hoc test are indicated. *P < 0.05; **P < 0.01. WT^{SGH}, single genotype housed WT animals; WT^{MGH}, mixed genotype housed animals. Test results with male animals that did not reach significance are presented in Extended Data Figure 6-1.

Figure 7. Behavioral alterations in the open field test in *Pcdh19* HET females and their WT littermates.

(A,B) Total distance travelled by females during the 20 minutes of the open field test at P21 (A) and P60 (B). (C,D) Distance travelled by females during the first 5 minutes of the open field test at P21 (C) and P60 (D). (E,F) Distance travelled by females during the second 5 minutes of the open field test at P21 (E) and P60 (F). Results correspond to the second day of testing at each age. For all panels, the upper axis shows the raw data points for each group. To their right, the gap in the line indicates the mean, and the lines extending vertically represent the standard deviation. The group and group sizes are indicated at the bottom. Note that each group appears twice in every graph, but with two different colors. The mean difference for each comparison is plotted in the lower axis as a bootstrap sampling distribution. The black dot represents the mean and the vertical bar it's 95% confidence interval. At the top of each graph the significance scores of the one-way ANOVA or Kruskal-Wallis test and their post-hoc test are indicated. *P < 0.05; **P < 0.01; ***P < 0.001. WT^{SGH}, single genotype housed WT animals; WT^{MGH}, mixed genotype housed animals. Test results with female animals for the open field and 24 h activity that did not reach significance are presented in Extended Data Figure 7-1.

Figure 8. Behavioral alterations in the EPM and social interaction tests in *Pcdh19* HET females and their WT littermates.

(A,B) Total time spent by females in the open arms of the elevated plus maze during the 5-minute test at P21 (A) and P60 (B). (C,D) Time spent by females interacting with a non-familiar female at P21 (C) and P60 (D). The total duration of the test was 5 minutes. For all panels, the upper axis shows the raw data points for each group. To their left, the gap in the line indicates the mean, and the lines extending vertically represent the standard deviation. The group and group sizes are indicated at the bottom. Note that each group appears twice in every graph, but with two different colors. The mean difference for each comparison is plotted in the lower axis as a bootstrap sampling distribution. The black dot represents the

mean and the vertical bar it's 95% confidence interval. At the top of each graph the significance scores of the one-way ANOVA or Kruskal-Wallis test and their post-hoc test are indicated. *P < 0.05; **P < 0.01; ***P < 0.001. WT^{SGH}, single genotype housed WT animals; WT^{MGH}, mixed genotype housed animals.

EXTENDED FIGURE LEGENDS

Figure 1-1

Gene expression and distribution of Pcdh19 in cortical excitatory projection neurons of the Allen Brain Atlas mouse Whole Cortex & Hippocampus - SMART-SEQ (2019) with 10X Smart-Seq Taxonomy (2020), represented by violin plots. The first row shows overall expression of Pcdh19 in the combined dataset excluding hippocampal regions for simplicity. Subsequent rows show expression by cortical region. Dots indicate the median value of the population. Absence of a violin plot in a row indicates none or fewer than 3 cells from that particular cortical region were mapped to the corresponding neuronal cluster. Black and red lines indicate consistent low and high expression of Pcdh19 across areas, respectively, asterisks highlight clusters with marked variation in Pcdh19 expression across cortical regions. ACA, anterior cingulate area; AI, agranular insular area; AUD, auditory areas; GU, gustatory areas; MOp, primary motor area; MOs-FRP, secondary motor area - frontal pole, cerebral cortex; ORB, orbital area; PL-ILA, prelimbic - infralimbic areas; PTLp, posterior parietal association areas; RSP, retrosplenial area; SSp, primary somatosensory area; SSs, supplemental somatosensory area; TEa-PERI-ECT, temporal association areas - perirhinal area - ectorhinal area; VIS, visual areas; VISp, primary visual area.

Figure 1-2

Gene expression and distribution of Pcdh19 in cortical inhibitory neurons of the Allen Brain Atlas mouse Whole Cortex & Hippocampus - SMART-SEQ (2019) with 10X Smart-Seq Taxonomy (2020), represented by violin plots. The first row shows overall expression of Pcdh19 in the combined dataset excluding hippocampal regions for simplicity. Subsequent rows show expression by cortical region. Dots indicate the median value of the population. Absence of a violin plot in a row indicates none or fewer than 3 cells from that particular cortical region were mapped to the corresponding neuronal cluster. Black and red lines

indicate consistent low and high expression of Pcdh19 across areas, respectively, asterisks highlight clusters with marked variation in Pcdh19 expression across cortical regions. ACA, anterior cingulate area; AI, agranular insular area; AUD, auditory areas; GU, gustatory areas; MOp, primary motor area; MOs-FRP, secondary motor area - frontal pole, cerebral cortex; ORB, orbital area; PL-ILA, prelimbic - infralimbic areas; PTLp, posterior parietal association areas; RSP, retrosplenial area; SSp, primary somatosensory area; SSs, supplemental somatosensory area; TEa-PERI-ECT, temporal association areas - perirhinal area - ectorhinal area; VIS, visual areas; VISp, primary visual area.

Figure 2-1

Gene expression and distribution of PCDH19 in cortical excitatory projection neurons of the Allen Brain Atlas human Multiple Cortical Areas dataset, represented by violin plots. The first row shows overall expression of PCDH19 in the combined dataset, subsequent rows show expression by brain region. Dots indicate the median value of the population. Absence of a violin plot in a row indicates none or fewer than 3 cells from that particular brain region were mapped to the corresponding neuronal subtype. Black and red lines indicate consistent low and high expression of PCDH19 across areas, respectively, asterisks highlight clusters with marked variation in PCDH19 expression across cortical regions. MTG, middle temporal gyrus; V1C, primary visual cortex; CgG, anterior cingulate gyrus; M1lm, primary motor cortex, lower limb region; S1ul primary somatosensory cortex upper limb region; S1lm, primary somatosensory cortex lower limb region; M1ul primary motor cortex, upper limb region, A1C, primary auditory cortex.

Figure 2-2

Gene expression and distribution of PCDH19 in cortical inhibitory neurons of the Allen Brain Atlas human Multiple Cortical Areas dataset, represented by violin plots. The first row shows

overall expression of PCDH19 in the combined dataset, subsequent rows show expression by brain region. Dots indicate the median value of the population. Absence of a violin plot in a row indicates none or fewer than 3 cells from that particular brain region were mapped to the corresponding neuronal subtype. Black and red lines indicate consistent low and high expression of PCDH19 across areas, respectively, asterisks highlight clusters with marked variation in PCDH19 expression across cortical regions. MTG, middle temporal gyrus; V1C, primary visual cortex; CgG, anterior cingulate gyrus; M1lm, primary motor cortex, lower limb region; S1ul primary somatosensory cortex upper limb region; S1lm, primary somatosensory cortex lower limb region; M1ul primary motor cortex, upper limb region, A1C, primary auditory cortex.

Figure 2-3

(A) Diagram indicating the existing correlations between ABA mouse and human cortical datasets. (B) Diagram showing the homology clusters defined by (Hodge et al. 2019) and the corresponding mouse and human neuronal subtypes assigned to each cluster for GABAergic neuronal clusters. (C) River plot showing the mapping of the nuclei from the MTG dataset to the subtypes defined by the Multiple Cortical Areas dataset, for inhibitory neurons.

Figure 6-1

(A) Total distance travelled in the open field by P60 males. (B) Distance travelled in the open field by P21 males, split into 5-minute intervals. The data for the first 5 minutes are shown in Figure 6. (C) Distance travelled in the open field by P60 males, split into 5-minute intervals. (D) Time spent by males in the center of the arena during the 20 minutes open field test at P21 and P60. (E) Time spent in the open arms of the elevated plus maze by P21 males. (F) Number of beam breaks during the 24 hour activity test for the males of the different

conditions. Light: light phase, dark: dark phase. (G) Number of beam breaks by hour in the 24 hour activity test for the males of the different conditions. The time of the day is shown on the X-axis and the grey square indicates the hours of the dark period. Numbers of tested animals were: 26 WTSGH, 18 WTMGH, 31 KO at P21 and 24 WTSGH, 18 WTMGH, 29 KO at P60. For the 24 hour activity test, number were 17 WTSGH, 10 WTMGH and 10 KO. Results are indicated as mean ± SEM. *P < 0.05. WTSGH, single genotype housed WT animals; WTMGH, mixed genotype housed animals.

Figure 6-2

(A,B) Distance travelled in the last two 5-minutes intervals of the open field test by P21 (A) and P60 (B) females. (C) Number of beam breaks during the 24 hour activity test for the females of the different conditions. Light: light phase, dark: dark phase. (D) Number of beam breaks by hour in the 24 hour activity test for the females of the different conditions. The time of the day is shown on the X-axis and the grey square indicates the hours of the dark period. (E,F) Time spent by females in the center of the arena during the 20 minutes open field test at P21 (E) and P60 (F). In these two panels, raw data are depicted in the upper axis, with the mean (gap) and standard deviation (vertical bars) to their right. Group and group sizes are indicated at the bottom. Note that each group appears twice in every graph, but in two different colors. The mean difference for each comparison is plotted in the lower axis as a bootstrap sampling distribution. The mean is indicated by the black dot and the 95% CI by the vertical bars. Numbers of tested animals were: 22 WTSGH, 29 WTMGH, 21 HET at P21 and P60. For the 24-hour activity test, number were 18 WTSGH, 11 WTMGH and 10 HET. Results are indicated as mean ± SEM. *P < 0.05. WTSGH, single genotype housed WT animals; WTMGH, mixed genotype housed animals.

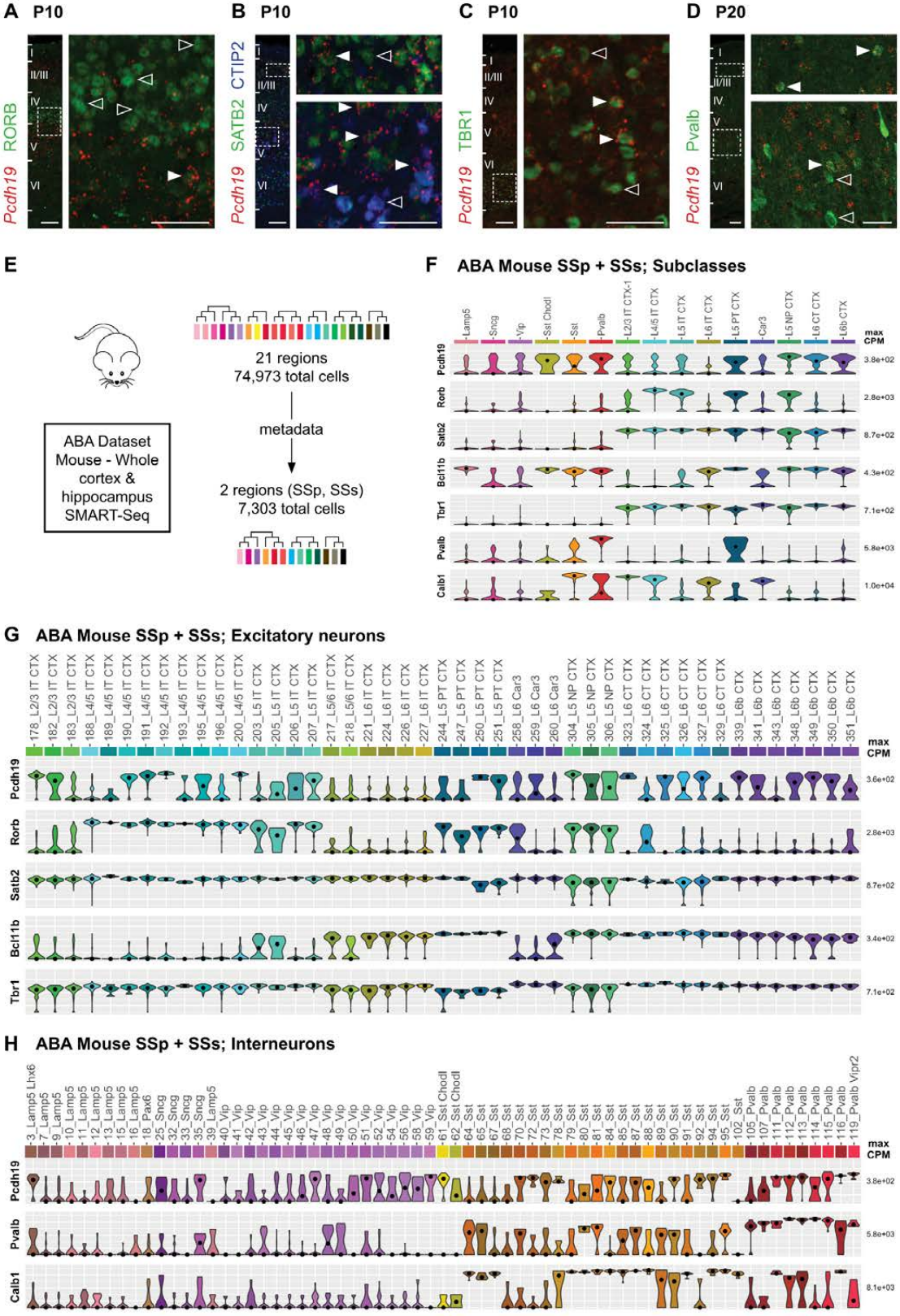

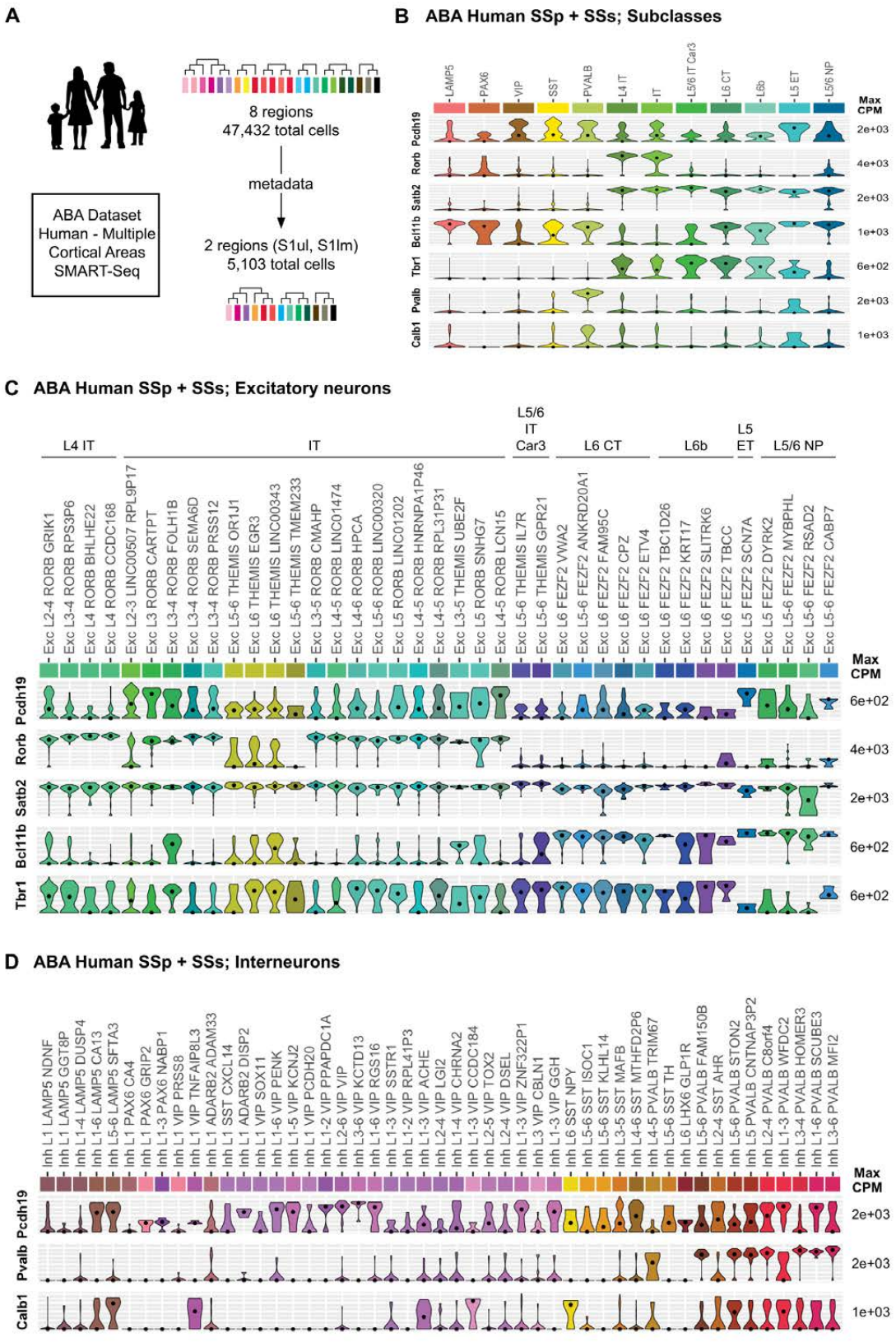

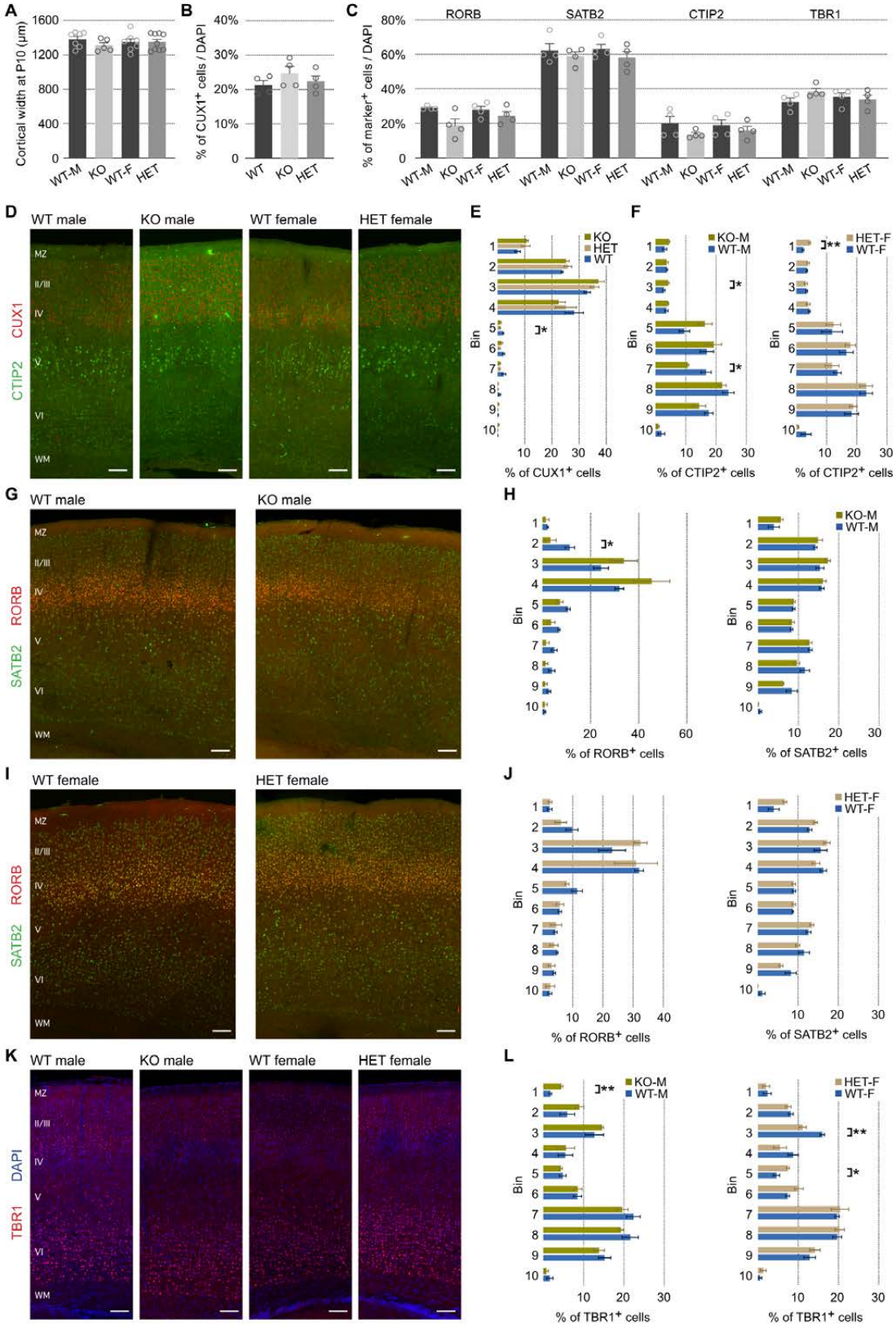

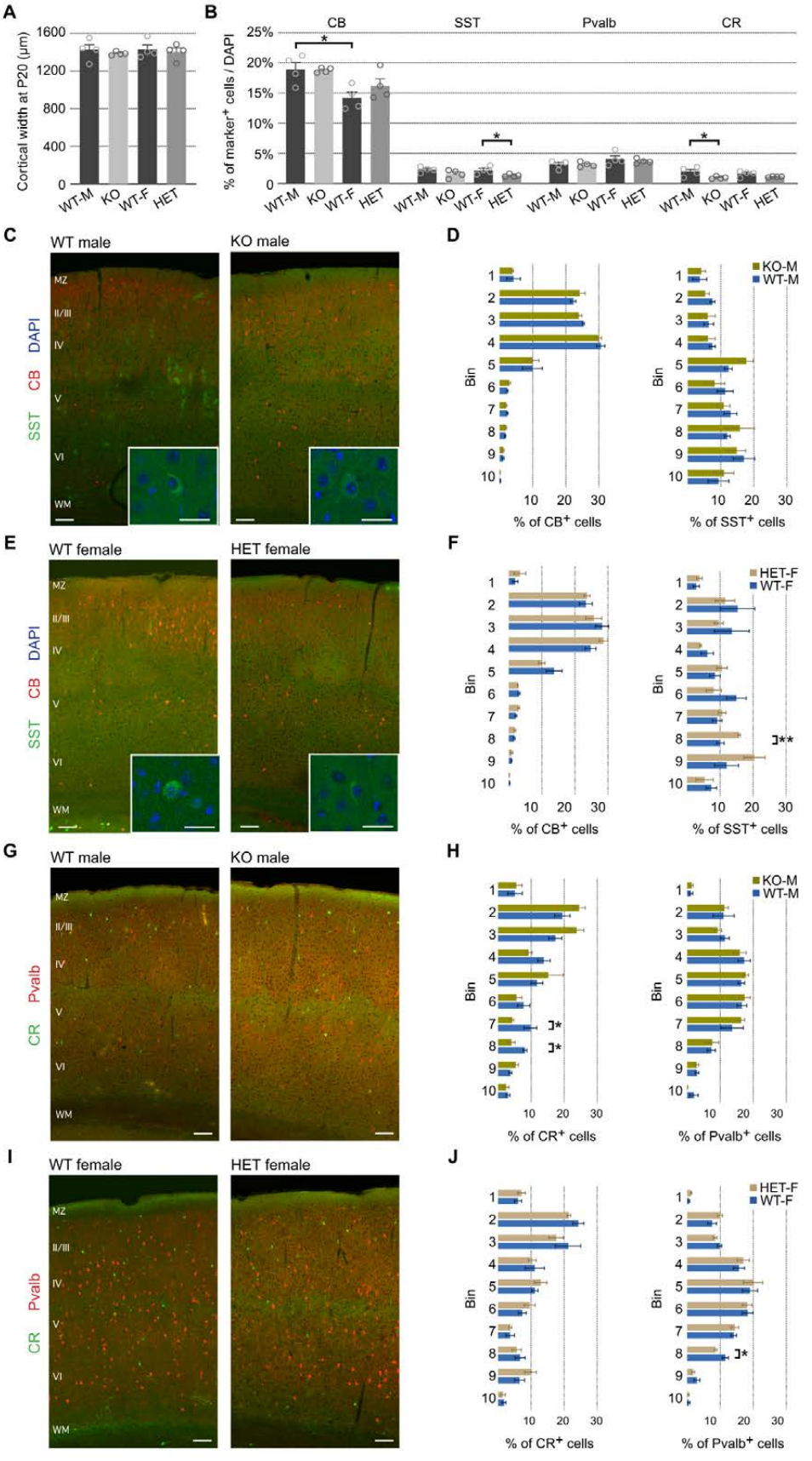

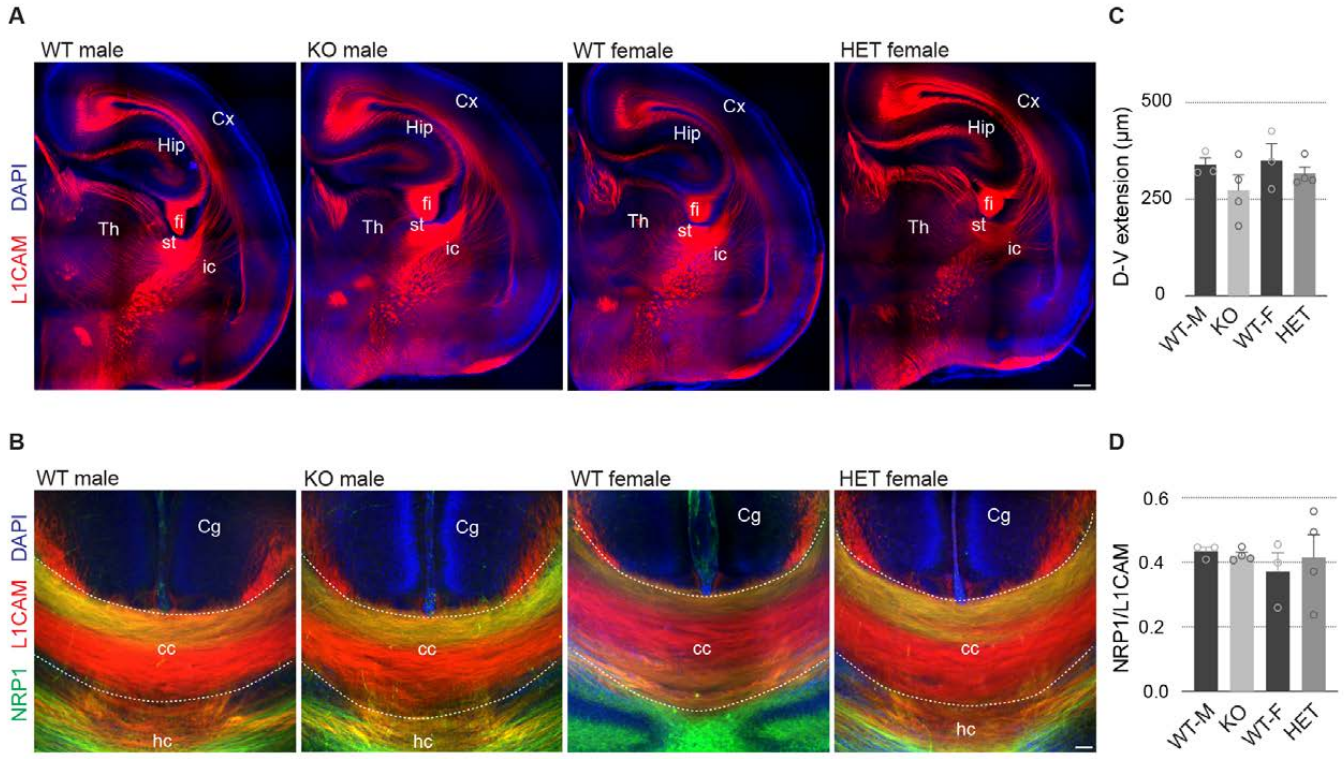

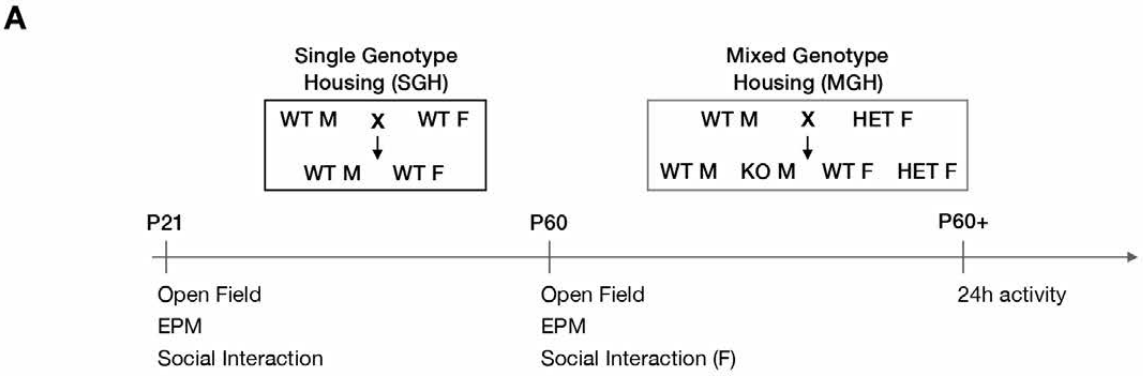

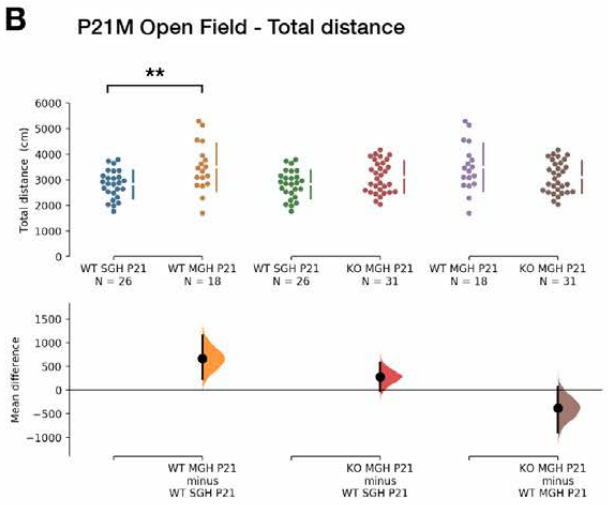

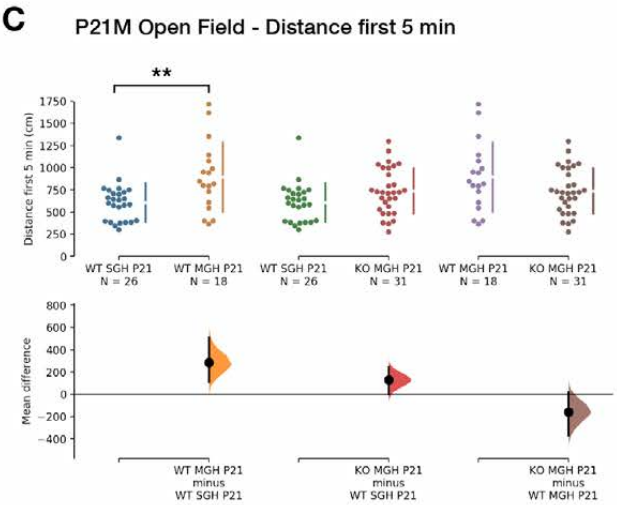

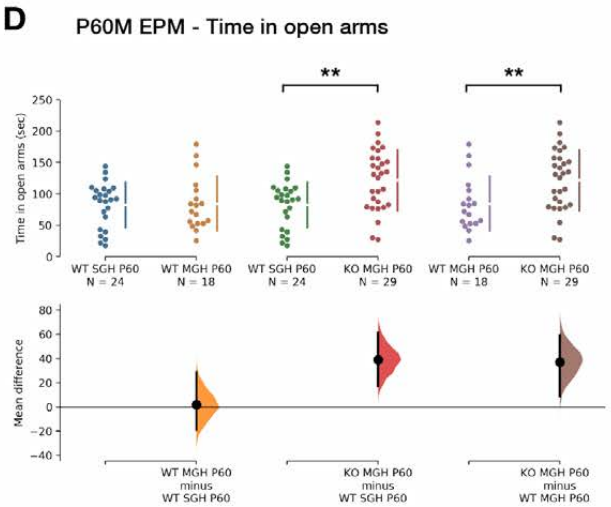

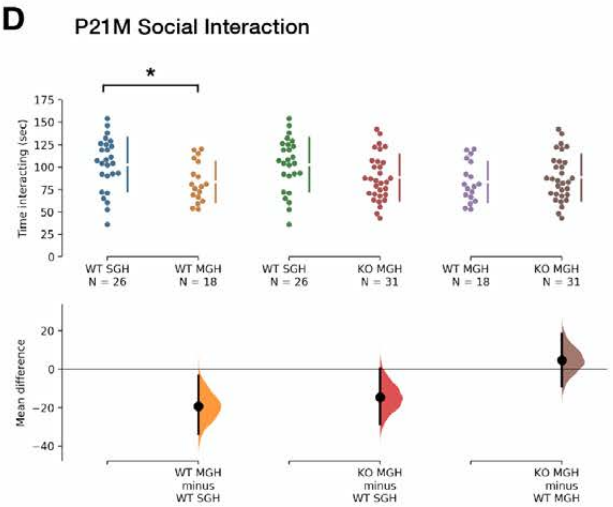

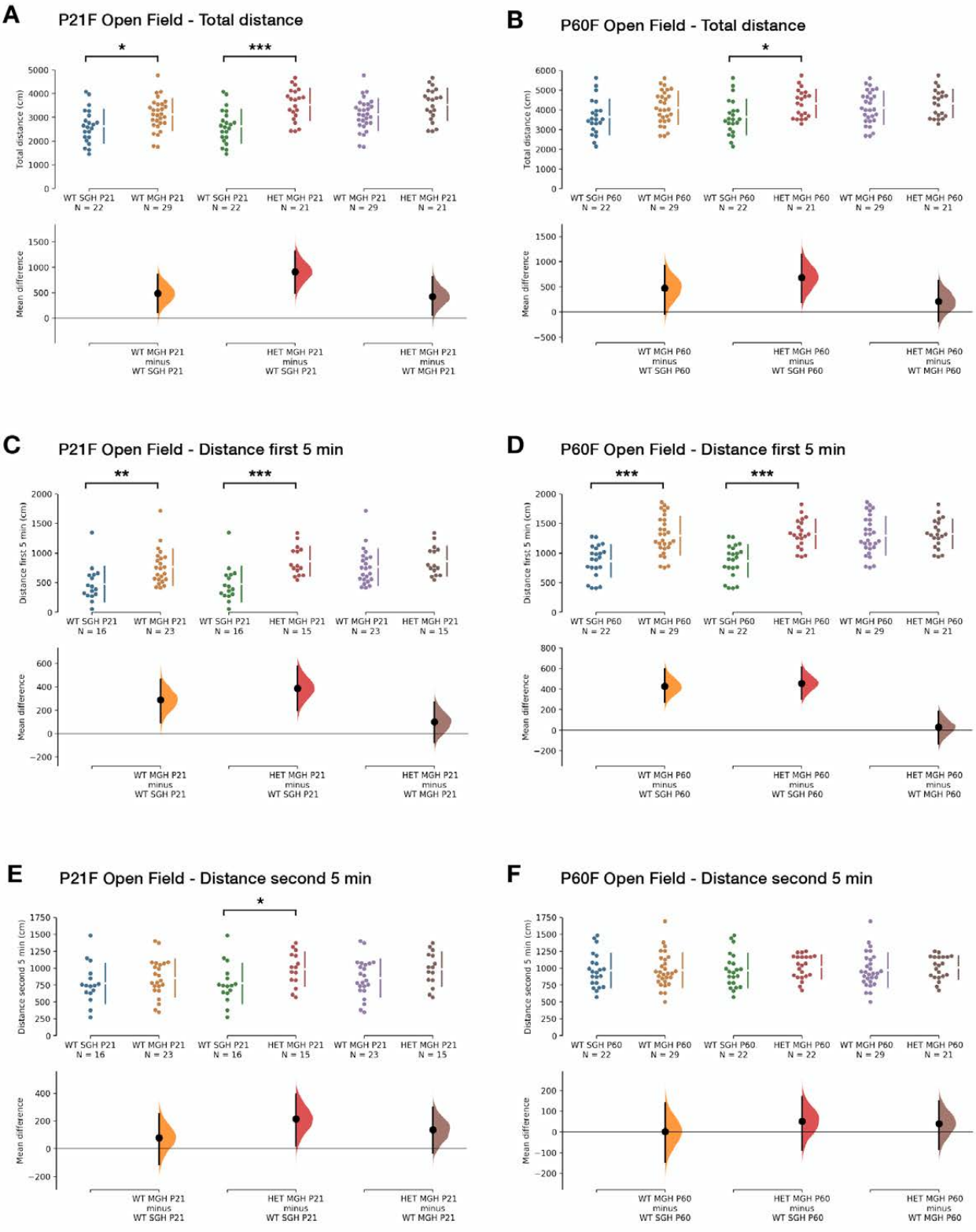

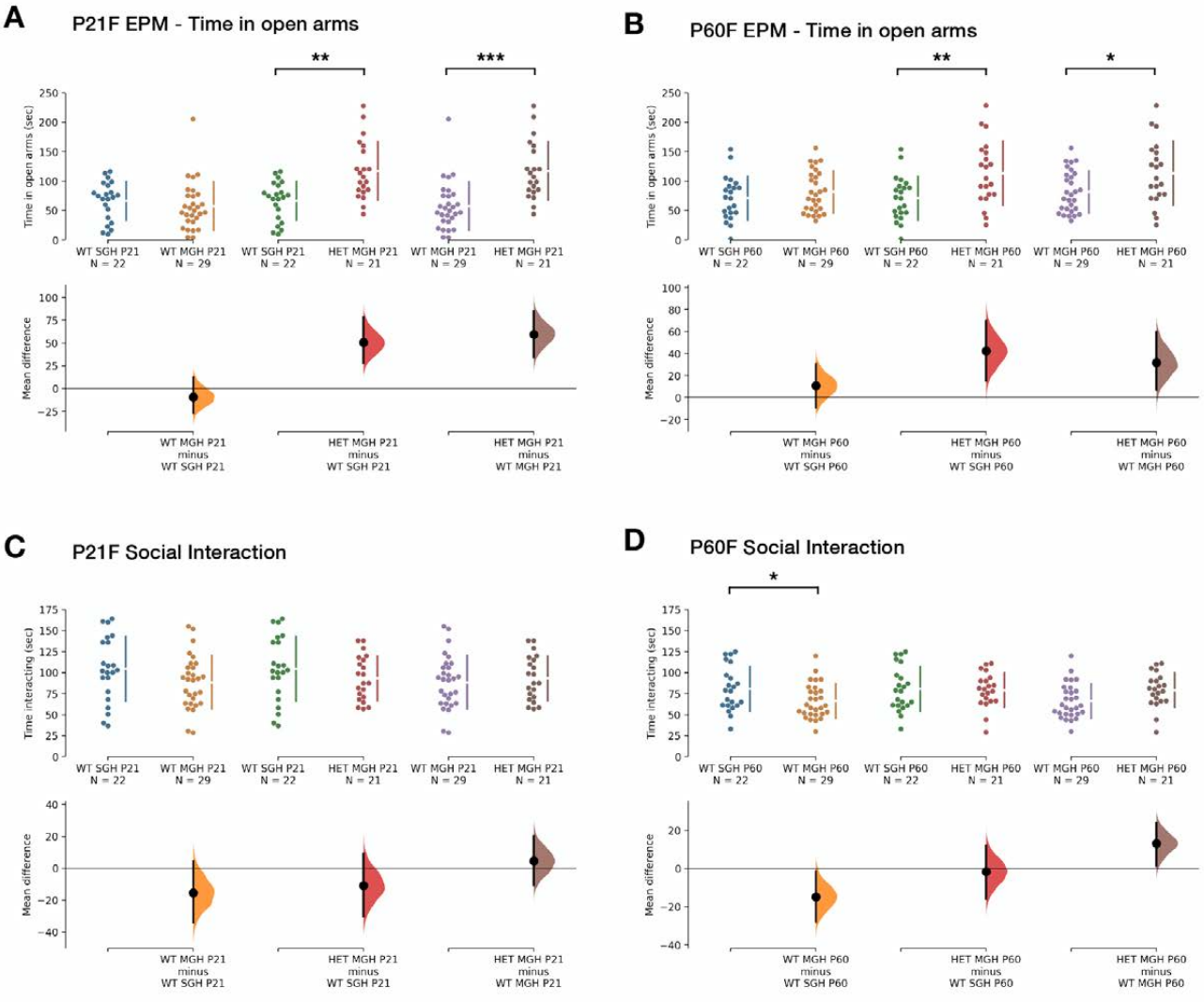

Table 1. Comparison of GABAergic clusters with high *Pcdh19* expression in mouse and human SSC

Mouse Whole Cortex & Hippocampus - SMART-SEQ (2019) with 10X-Smart-Seq Taxonomy (2020)	Mouse V1 & ALM - SMART-SEQ (2018)	Homologous cell type taxonomy (Hodge et al 2019)	Human MTG - SMART-SEQ (2018)	Human MULTIPLE CORTICAL AREAS - SMART-SEQ (2019)
3_Lamp5 Lhx6 (H)	Lamp5 Lhx6	Lamp5 Lhx6	Inh L2-5 LAMP5 CA1	Inh L1-6 LAMP5 CA13 (H) Inh L5-6 LAMP5 SFTA3 (H)
25_Sncg (M-H) 35_Sncg (H)	Sncg Vip Nptx2 Sncg Gpr50 Sncg Vip Itih5	Vip Sncg	Inh L1-2 VIP TSPAN12	Inh L1 VIP PRSS8 (L)
40-41_Vip (L) 44-47_Vip (L)	Serpinf Aqp5 Vip Vip Pygm C1ql1 Vip Chat Htr1f	Vip 3	Inh L1-2 VIP PCDH20	Inh L1-2 VIP PPAPDC1A (H)
47_Vip (H)	Vip Rspo4 Rxfp1 Chat Vip Rspo1 Itga4	Vip 4	Inh L2-4 VIP CBLN1 Inh L1-3 VIP CCDC184 Inh L1-3 VIP GGH Inh L1-3 VIP CHRM2	Inh L3 VIP CBLN1 (L) Inh L1-3 VIP ACHE (M) Inh L1-3 VIP GGH (H) Inh L1-2 VIP ZNF322P1 (H)
51_Vip (H)	Vip Gpc3 Slc18a3	Vip 2	Inh L2-6 VIP QPCT Inh L3-6 VIP HS3ST3A1	Inh L1-6 VIP RGS16 (H) Inh L2-6 VIP VIP (H) Inh L3-6 VIP KCTD13 (H)
59_Vip (H)	Vip Igfbp6 Car10	Vip 1	Inh L1-4 VIP PENK Inh L1-3 VIP ADAMTSL1 Inh L1-2 SST BAGE2	Inh L1-6 VIP PENK (H) Inh L1-5 VIP KCNJ2 (H) Inh L1 VIP CXCL14 (L) Inh L1 ADARB2 DISP2 (H)
61_Sst Chodl (H)	Sst Chodl	Sst Chodl	Inh L3-6 SST NPY	Inh L6 SST NPY (M)
64_Sst (L) 66_Sst (N.P.) 67_Sst (L) 79_Sst (L) 80-82_Sst (M)	Sst Myh8 Fibin Sst Chrna2 Glra3 Sst Myh8 Etv1 Sst Nr2f2 Necab1 Sst Chrna2 Ptgdr	Sst 1	Inh L3-6 SST HPGD Inh L4-6 SST B3GAT2	Inh L4-6 SST MTHFD2P6 (M)

Mouse Whole Cortex & Hippocampus - SMART-SEQ (2019) with 10X-Smart-Seq Taxonomy (2020)	Mouse V1 & ALM - SMART-SEQ (2018)	Homologous cell type taxonomy (Hodge et al 2019)	Human MTG - SMART-SEQ (2018)	Human MULTIPLE CORTICAL AREAS - SMART-SEQ (2019)
70_Sst (H) 72_Sst (H) 73_Sst (H) 78_Sst (H)	Sst Tac2 Tacstd2 Sst Rxfp1 Eya1 Sst Rxfp1 Prdm8	Sst 3	Inh L4-6 SST GXYLT2 Inh L5-6 SST NPM1P10	Inh L5-6 SST KLHL14 (L) Inh L5-6 SST ISOC1 (L)
84_Sst (H)	Sst Esm1	Sst 2	Inh L5-6 SST KLHDC8A (only 3 cells)	no equivalent
90_Sst (H) 92_Sst (H) 94_Sst (H) 95_Sst (H)	Sst Calb2 Pdlim5 Sst Tac1 Tacr3 Sst Calb2 Necab1 Sst Tac1 Htr1d	Sst 5	Inh L1-3 SST CALB1	Inh L3-5 SST MAFB (M)
111_Pvalb (H)	Pvalb Akr1c18 Ntf3	Pvalb 1	Inh L5-6 PVALB LGR5 Inh L5-6 SST TH Inh L4-5 PVALB MEPE Inh L5-6 SST MIR548F2	Inh L5-6 PVALB FAM150B (M) Inh L5-6 SST TH (M) Inh L5 PVALB CNTNAP3P2 (M) Inh L5-6 PVALB STON2 (M)
	Pvalb Sema3e Kank4 Palb Calb1 Sst	Pvalb 2	Inh L2-4 PVALB WFDC2 Inh L4-6 PVALB SULF1	Inh L2-4 PVALB C8ORF4 (M) Inh L5 PVALB CNTNAP3P2 (M) Inh L1-3 PVALB WFDC2 (H) Inh L3-4 PVALB HOMER3 (L)
112_Pvalb (H)	Pvalb Gpr149 Islr	Pvalb 1	Inh L5-6 PVALB LGR5 Inh L5-6 SST TH Inh L4-5 PVALB MEPE Inh L5-6 SST MIR548F2	Inh L5-6 PVALB FAM150B (M) Inh L5-6 SST TH (M) Inh L5 PVALB CNTNAP3P2 (M) Inh L5-6 PVALB STON2 (M)
113_Pvalb (H) 114_Pvalb (M) 115_Pvalb (H)	Pvalb Tpbg Pvalb Reln Tac1 Pvalb Reln Itm2a	Pvalb 2	Inh L2-4 PVALB WFDC2 Inh L4-6 PVALB SULF1	Inh L2-4 PVALB C8ORF4 (M) Inh L5 PVALB CNTNAP3P2 (M) Inh L1-3 PVALB WFDC2 (H) Inh L3-4 PVALB HOMER3 (L)

Mouse Whole Cortex & Hippocampus - SMART-SEQ (2019) with 10X-Smart-Seq Taxonomy (2020)	Mouse V1 & ALM - SMART-SEQ (2018)	Homologous cell type taxonomy (Hodge et al 2019)	Human MTG - SMART-SEQ (2018)	Human MULTIPLE CORTICAL AREAS - SMART-SEQ (2019)
116_Pvalb (H)	Sst Tac1 Tacr3 Sst Tac1 Htr1d	Sst 5	Inh L1-3 SST CALB1	Inh L3-5 SST MAFB (M)
	Palb Calb1 Sst Pvalb Tpbg	Pvalb 2	Inh L2-4 PVALB WFDC2 Inh L4-6 PVALB SULF1	Inh L2-4 PVALB C8ORF4 (M) Inh L5 PVALB CNTNAP3P2 (M) Inh L1-3 PVALB WFDC2 (H) Inh L3-4 PVALB HOMER3 (L)
119_Pvalb (H)	Pvalb Vipr2	Chandelier	Inh L2-5 PVALB SCUBE3	Inh L1-6 PVALB SCUBE3 (H)

Table 2. Statistical analysis of cortical width and marker composition at P10.

Data	Comparison (n)	Data structure (normality?)	Equal variance?	Test	Results
Cortical width (a)	WT-M (7) vs KO-M (5)	yes	yes	unpaired t-test	$t_{(2,10)} = 1.495$ $P = 0.1658$
	WT-F (7) vs HET-F (9)	no	yes	Mann-Whitney	$U = 31$ $P > 0.9999$
	WT-M (7) vs WT-F (7)	yes	yes	unpaired t-test	$t_{(2,12)} = 0.6648$ $P = 0.5187$
% CUX1 over DAPI (b)	WT (4) vs KO (4) vs HET (4)	yes	yes	one-way ANOVA	$F_{(2,9)} = 1.065$ $P = 0.3846$
% RORB over DAPI (c)	WT-M (4) vs KO-M (4)	no	yes	Mann-Whitney	$U = 3$ $P = 0.2$
	WT-F (4) vs HET-F (4)	yes	yes	unpaired t-test	$t_{(2,6)} = 1.060$ $P = 0.3301$
	WT-M (4) vs WT-F (4)	no	yes	Mann-Whitney	$U = 7$ $P = 0.8857$
% SATB2 over DAPI (d)	WT-M (4) vs KO-M (4)	yes	yes	unpaired t-test	$t_{(2,6)} = 0.6827$ $P = 0.5203$
	WT-F (4) vs HET-F (4)	yes	yes	unpaired t-test	$t_{(2,6)} = 1.105$ $P = 0.3113$
	WT-M (4) vs WT-F (4)	yes	yes	unpaired t-test	$t_{(2,6)} = 0.1644$ $P = 0.8749$
% CTIP2 over DAPI (e)	WT-M (4) vs KO-M (4)	yes	yes	unpaired t-test	$t_{(2,6)} = 1.557$ $P = 0.1704$
	WT-F (4) vs HET-F (4)	yes	yes	unpaired t-test	$t_{(2,6)} = 0.7295$ $P = 0.4932$
	WT-M (4) vs WT-F (4)	yes	yes	unpaired t-test	$t_{(2,6)} = 0.2306$ $P = 0.8253$
% TBR1 over DAPI (f)	WT-M (4) vs KO-M (4)	no	yes	Mann-Whitney	$U = 1$ $P = 0.0571$
	WT-F (4) vs HET-F (4)	yes	yes	unpaired t-test	$t_{(2,6)} = 0.3816$ $P = 0.7159$
	WT-M (4) vs WT-F (4)	yes	yes	unpaired t-test	$t_{(2,6)} = 0.8509$ $P = 0.4275$

Table 3. Statistical analysis of cortical width and marker composition at P20.

Data	Comparison (n)	Data structure (normality?)	Equal variance?	Test	Results
Cortical width (a)	WT-M (4) vs KO-M (4)	yes	no	Welch's t-test	$t_{(2,3.179)} = 0.6456$ $P = 0.1658$
	WT-F (4) vs HET-F (4)	yes	yes	unpaired t-test	$t_{(2,6)} = 0.4098$ $P = 0.6962$
	WT-M (4) vs WT-F (4)	yes	yes	unpaired t-test	$t_{(2,6)} = 0.06806$ $P = 0.9480$
% CB over DAPI (b)	WT-M (4) vs KO-M (4)	yes	no	Welch's t-test	$t_{(2,3.168)} = 0.1169$ $P = 0.9140$
	WT-F (4) vs HET-F (4)	yes	yes	unpaired t-test	$t_{(2,6)} = 1.291$ $P = 0.2443$
	WT-M (4) vs WT-F (4)	yes	yes	unpaired t-test	$t_{(2,6)} = 3.054$ $P = 0.0224$
% SST over DAPI (c)	WT-M (4) vs KO-M (4)	yes	yes	unpaired t-test	$t_{(2,6)} = 1.733$ $P = 0.1339$
	WT-F (4) vs HET-F (4)	yes	yes	unpaired t-test	$t_{(2,6)} = 2.578$ $P = 0.0419$
	WT-M (4) vs WT-F (4)	yes	yes	unpaired t-test	$t_{(2,6)} = 0.3061$ $P = 0.7698$
% PVALB over DAPI (d)	WT-M (4) vs KO-M (4)	yes	yes	unpaired t-test	$t_{(2,6)} = 0.01984$ $P = 0.9848$
	WT-F (4) vs HET-F (4)	yes	yes	unpaired t-test	$t_{(2,6)} = 0.6266$ $P = 0.5540$
	WT-M (4) vs WT-F (4)	yes	yes	unpaired t-test	$t_{(2,6)} = 1.421$ $P = 0.2051$
% CR over DAPI (e)	WT-M (4) vs KO-M (4)	yes	yes	unpaired t-test	$t_{(2,6)} = 0.0459$ $P = 2.509$
	WT-F (4) vs HET-F (4)	yes	no	Welch's t-test	$t_{(2,3.172)} = 2.026$ $P = 0.1308$
	WT-M (4) vs WT-F (4)	yes	yes	unpaired t-test	$t_{(2,6)} = 0.7616$ $P = 0.4752$

Table 4. Statistical analysis of dorso-ventral extension and NRP1/L1CAM ratio in the *corpus callosum* of wild-type and Pcdh19 mutant pups.

Data	Comparison (n)	Data structure (normality?)	Equal variance?	Test	Results
D-V extension (a)	WT-M (3) vs KO-M (4)	yes	yes	unpaired t-test	$t_{(2,5)} = 1.338$ $P = 0.2385$
	WT-F (3) vs HET-F (4)	no	yes	Mann-Whitney	$U = 5$ $P = 0.8571$
	WT-M (3) vs WT-F (3)	yes	yes	unpaired t-test	$t_{(2,4)} = 0.2420$ $P = 0.8206$
NRP1/L1CAM ratio (b)	WT-M (3) vs KO-M (4)	no	yes	Mann-Whitney	$U = 5$ $P = 0.8571$
	WT-F (3) vs HET-F (4)	yes	yes	unpaired t-test	$t_{(2,5)} = 0.4525$ $P = 0.6699$
	WT-M (3) vs WT-F (3)	no	yes	Mann-Whitney	$U = 3$ $P = 0.7000$

Table 5. Statistical analysis of the behavioral experiments in P21 and adult males.

Behavioral Test	Sex	Age	normal data?	equal variance?	Test	Results
Open Field – Total distance Day 2	M	P21	yes	yes	one-way ANOVA	$F_{(2, 72)} = 5.017$ $P = 0.0091$ Post hoc Tukey: WT^{SGH} vs WT^{MGH} $P = 0.0063$ WT^{SGH} vs KO $P = 0.2796$ WT^{MGH} vs KO $P = 0.1468$
Open Field – Total distance Day 2	M	P60	yes	yes	one-way ANOVA	$F_{(2, 68)} = 1.13$ $P = 0.329$
Open Field - Intervals Day 2 - 0-5min	M	P21	no	yes	Kruskal Wallis	$H_{(2)} = 9.354$ $P = 0.0093$ Post hoc Dunn's: WT^{SGH} vs WT^{MGH} $P = 0.0079$ WT^{SGH} vs KO $P = 0.1711$ WT^{MGH} vs KO $P = 0.4797$
Open Field - Intervals Day 2 - 5-10min	M	P21	yes	yes	one-way ANOVA	$F_{(2, 72)} = 0.719$ $P = 0.491$
Open Field - Intervals Day 2 - 10-15min	M	P21	yes	yes	one-way ANOVA	$F_{(2, 72)} = 0.976$ $P = 0.382$
Open Field - Intervals Day 2 - 15-20min	M	P21	yes	yes	one-way ANOVA	$F_{(2, 72)} = 2.184$ $P = 0.12$
Open Field - Intervals Day 2 - 0-5min	M	P60	yes	yes	one-way ANOVA	$F_{(2, 68)} = 1.312$ $P = 0.276$
Open Field - Intervals Day 2 - 5-10min	M	P60	yes	yes	one-way ANOVA	$F_{(2, 68)} = 1.292$ $P = 0.2813$
Open Field - Intervals Day 2 - 10-15min	M	P60	yes	yes	one-way ANOVA	$F_{(2, 68)} = 0.13$ $P = 0.879$
Open Field - Intervals Day 2 - 15-20min	M	P60	no	yes	Kruskal Wallis	$H_{(2)} = 1.56$ $P = 0.4584$
Open Field – Time in centre Day 2	M	P21	no	yes	Kruskal Wallis	$H_{(2)} = 2.7579$ $P = 0.2518$
Open Field – Time in centre Day 2	M	P60	no	yes	Kruskal Wallis	$H_{(2)} = 3.2761$ $P = 0.1671$

Behavioral Test	Sex	Age	normal data?	equal variance?	Test	Results
24 h activity - total	M	> P60	yes	yes	one-way ANOVA	$F_{(2, 34)} = 0.4831$ $P = 0.6210$
24 h activity – light period	M	> P60	yes	yes	one-way ANOVA	$F_{(2, 34)} = 3.031$ $P = 0.0615$
24 h activity – dark period	M	> P60	yes	yes	one-way ANOVA	$F_{(2, 34)} = 0.3135$ $P = 0.7330$
Elevated Plus Maze	M	P21	yes	yes	one-way ANOVA	$F_{(2, 72)} = 1.994$ $P = 0.144$
Elevated Plus Maze	M	P60	yes	yes	one-way ANOVA	$F_{(2, 68)} = 6.879$ $P = 0.0019$ Post hoc Tukey: WT^{SGH} vs WT^{MGH} $P = 0.9893$ WT^{SGH} vs KO $P = 0.0042$ WT^{MGH} vs KO $P = 0.0138$
Social interaction	M	P21	yes	yes	one-way ANOVA	$F_{(2, 72)} = 2.911$ $P = 0.039$ Post hoc Dunnet's (all vs WT SGH): WT^{SGH} vs WT^{MGH} $P = 0.0382$ WT^{SGH} vs KO $P = 0.0771$

Table 5. Statistical analysis of the behavioral experiments in P21 and adult females.

Behavioral Test	Sex	Age	normal data?	equal variance?	Test	Results
Open Field – Total distance Day 2	F	P21	yes	yes	one-way ANOVA	$F_{(2, 69)} = 9.539$ $P = 0.0002$ Post hoc Tukey: WT^{SGH} vs WT^{MGH} $P = 0.0382$ WT^{SGH} vs HET $P = 0.0001$ WT^{MGH} vs HET $P = 0.0837$
Open Field – Total distance Day 2	F	P60	yes	yes	one-way ANOVA	$F_{(2, 69)} = 3.990$ $P = 0.0229$ Post hoc Tukey: WT^{SGH} vs WT^{MGH} $P = 0.1094$ WT^{SGH} vs HET $P = 0.0214$ WT^{MGH} vs HET $P = 0.6459$
Open Field - Intervals Day 2 - 0-5min	F	P21	no	yes	Kruskal Wallis	$H_{(2)} = 21.86$ $P < 0.0001$ Post hoc Dunn's: WT^{SGH} vs WT^{MGH} $P = 0.0055$ WT^{SGH} vs HET $P < 0.0001$ WT^{MGH} vs HET $P = 0.2018$
Open Field - Intervals Day 2 - 5-10min	F	P21	yes	yes	one-way ANOVA	$F_{(2, 69)} = 3.290$ $P = 0.0432$ Post hoc Tukey: WT^{SGH} vs WT^{MGH} $P = 0.5888$ WT^{SGH} vs HET $P = 0.0359$ WT^{MGH} vs HET $P = 0.2036$
Open Field - Intervals Day 2 - 10-15min	F	P21	yes	yes	one-way ANOVA	$F_{(2, 69)} = 2.102$ $P = 0.13$
Open Field - Intervals Day 2 - 15-20min	F	P21	yes	yes	one-way ANOVA	$F_{(2, 69)} = 1.038$ $P = 0.36$
Open Field - Intervals Day 2 - 0-5min	F	P60	yes	yes	one-way ANOVA	$F_{(2, 69)} = 17.95$ $P < 0.0001$ Post hoc Tukey: WT^{SGH} vs WT^{MGH} $P < 0.0001$ WT^{SGH} vs HET $P < 0.0001$ WT^{MGH} vs HET $P = 0.9276$
Open Field - Intervals Day 2 - 5-10min	F	P60	yes	yes	one-way ANOVA	$F_{(2, 69)} = 0.228$ $P = 0.797$
Open Field - Intervals Day 2 - 10-15min	F	P60	yes	yes	one-way ANOVA	$F_{(2, 69)} = 1.068$ $P = 0.349$
Open Field - Intervals Day 2 - 15-20min	F	P60	no	yes	Kruskal Wallis	$H_{(2)} = 3.2334$ $P = 0.1986$

Behavioral Test	Sex	Age	normal data?	equal variance?	Test	Results
Open Field – Time in centre Day 2	F	P21	no	yes	Kruskal Wallis	$H_{(2)} = 4.6819$ $P = 0.0962$
Open Field – Time in centre Day 2	F	P60	no	yes	Kruskal Wallis	$H_{(2)} = 4.0863$ $P = 0.1296$
24 h activity - total	F	> P60	yes	yes	one-way ANOVA	$F_{(2, 36)} = 1.077$ $P = 0.3512$
24 h activity – light period	F	> P60	yes	yes	one-way ANOVA	$F_{(2, 36)} = 2.290$ $P = 0.1159$
24 h activity – dark period	F	> P60	yes	yes	one-way ANOVA	$F_{(2, 36)} = 1.103$ $P = 0.3429$
Elevated Plus Maze	F	P21	no	yes	Kruskal Wallis	$H_{(2)} = 20.943$ $P < 0.001$ Post hoc Dunn's: WT^{SGH} vs WT^{MGH} $P = 0.8101$ WT^{SGH} vs HET $P = 0.0042$ WT^{MGH} vs HET $P < 0.0001$
Elevated Plus Maze	F	P60	yes	yes	one-way ANOVA	$F_{(2, 69)} = 5.085$ $P = 0.0041$ Post hoc Tukey: WT^{SGH} vs WT^{MGH} $P = 0.5689$ WT^{SGH} vs HET $P = 0.0043$ WT^{MGH} vs HET $P = 0.0401$
Social interaction	F	P21	yes	yes	one-way ANOVA	$F_{(2, 69)} = 1.297$ $P = 0.2425$
Social interaction	F	P60	yes	yes	one-way ANOVA	$F_{(2, 69)} = 3.536$ $P = 0.0398$ Post hoc Dunnet's (all vs WT SGH): WT^{SGH} vs WT^{MGH} $P = 0.0432$ WT^{MGH} vs HET $P = 0.9654$